KTH Chemical Science
and Engineering

On the aqueous reactions of the aminyl radicalwith molecular oxygen and the superoxide anion

BJÖRN DAHLGREN

Master's Thesis, School of Chemical Science and Engineering, KTH Royal Institute of Technology
Supervisor: Prof. Tore Brinck[a]
Examiner: Prof. Johan Lind[b]

Abstract

Two key routes of the oxidation of ammonia is the reaction between the aminyl radical with molecular oxygen and superoxide. Fundamental insights in its oxidation is of great importance to both our understanding of atmospheric chemistry, biological effects as well as the safety assessments in nuclear industry. The gas phase reactions differ largely in rate compared to the aqueous reactions. In this work, the mechanism for the aqueous reactions have been studied computationally using ab initio quantum chemical calcultions. Reaction barriers have been quantified and compared with experimental data in the litterature. Also, the absorbtion spectrum of one of the postulated intermediates is verified using TDDFT. Furthermore, γ-radiolysis experiments have been conducted to test a model for aqueous radical oxidation of ammonia by investigating the yield of one of the final products, peroxynitrite. The model consists of a large part of reported reactions relevant to the aqueous radiolysis of nitrogen containing solutions (with an emphasis on ammonia). The dependence of the yield on the chosen experimental conditions is compared to that calculated using the model.

The results of the quantum chemical computations for the reaction with oxygen is in agreement with earlier experimentally reported absorption spectrum and rate of decomposition of a key intermediate, the aminyl peroxide radical. Both properties, however, only agree when a large enough number of explicit water molecules are included in the computations. The dependence of the results on the chosen number of water molecules as well as the level of theory is discussed. The evaluation of the model for radiolysis of aqueous ammonia shows that the current understanding of oxygenated systems where superoxide is in excess with respect to hydroxyl radical is good. For systems deficient in superoxide, the model fails to accurately predict the yield of the final product under investigation, peroxynitrite, and it raises the question whether some unknown process has been overlooked in earlier studies.

Referat

Insikter i aminylradikalens vattenfasreaktioner med syrgas och superoxidanjonen

Två huvudvägar för oxidationen av ammoniak är reaktionen mellan aminyl radikalen och syrgas, samt med superoxidanjonen. Fundamenala insikter i dess oxidation är mycket viktiga både för vår förståelse av atmosfärkemi, biologiska effekter samt säkerhetsbedömningar inom det kärntekniska området. Gasfas reaktionerna skiljer sig vida med avseende på hastighet från vattenfas reaktionerna. I detta arbete har mekanismen för vattenfas reaktionerna studerats med kvantkemiska beräkningar. Reaktionsbarriärer har kvantifierats och jämförts med experimentella data rapporterade tidigare. Dessutom har absorptionsspektrumet för en postulerad nyckelintermediär verifierats genom TDDFT beräkningar. Vidare har experiment med γ-radiolys genomförts för att utvärdera en modell för radikal oxidationen av ammoniak i vattenfas, överensstämmelsen mellan modell och experiment undersöktes för mängden bildad peroxynitrit. Modellen består av ett stort antal tidigare rapporterade reaktioner relevanta för radiolysen av vattenlösningar av enkla kväveföreningar (med tyngdpunk på ammoniak). Utbytets beroende på valda experimentella förutsättningar jämförs med vad modellen förutsäger. Resultaten av de kvantkemiska beräkningarna för reaktionen med syrgas är i överensstämmelse med tidigare rapporterade absorptionsspektrum och sönderfallshastighet för en nyckelintermediär, aminylperoxidradikalen. Båda egenskaperna överensstämmer dock endast ifall ett tillräckligt stort antal vatten molekyler inkluderas i beräkningarna. En diskussion förs kring resultatens beroende av valt antal vattenmolekyler liksom nivå på den teoretiska behandlingen. Utvärderingen av modellen för radiolys av vattenlösningar av ammoniak visar att den nuvarande kunskapsnivån för syresatta system, där superoxid bildas i överskott, är god. För system där hydroxylradikalen är i överskott förmår modellen ej att förutsäga verkligt utbyte av peroxynitrit, vilket väcker frågan hurvida en hittills okänd mekanism kan ha förbisetts i tidigare studier.

Contents

List of Figures

List of Tables

Preface

This MSc Thesis is divided into two chapters. In the first chapter, the reader is introduced to the theoretical and experimental tools used in this work. The second chapter, which assumes some familiarity with the concepts introduced in the first chapter, then presents the specific scientific problem investigated, its findings, how it relates to earlier efforts and what conclusions can be made.

Chapter 1

Theoretical background

This chapter gives a brief overview of the theoretical background needed for the understanding of the methods and for the interpretation of obtained results presented in chapter 2.

1.1 Computational chemistry

Chemistry can essentially be described as the interaction between electrons and nuclei, and chemical reactions more specifically, as the rearrangement of nuclei within (intramolecular) and between (intermolecular) stable constellations of nuclei (molecules), i.e. the breaking and forming of chemical bonds.

Quantum Chemistry (QC) is the field which explores chemical phenomena by computing molecular properties from first principles (*ab initio* methods) with no or very few parameters. Thanks to the so far exponential increase in computational performance it is today possible to calculate electronic structure properties for large molecules and molecular systems. The larger the system is, the more simplifications and approximations are needed in order to make the computations realizable. Within computational chemistry one often talks of chemical accuracy, i.e. a numerical accuracy good enough to predict phenomena within the field of chemistry (these may be qualitative for some properties and quantitative for others).

In this work chemical rates of reactions have been investigated. Usually one does not strive for quantitative agreement of rate constants with experiments. This is because the activation energy can only be estimated within approximately $10\,\mathrm{kJ\,mol^{-1}}$,[1] rendering the uncertainty at *e.g.* 298.15 K to be a factor of ~50. So the expectation is to investigate the compatibility of computed barriers with proposed mechanisms and observed experimental data.

1.1.1 The Schrödinger equation

In order to theoretically model the interaction between electrons and nuclei, the electrons need to be accurately described. The low mass of the electron renders any

attempt of applying classical mechanics futile. Instead we need to apply quantum mechanics.

The time-dependent Schrödinger equation[2] is given as:

$$i\hbar\frac{\partial}{\partial t}\Psi_n(\mathbf{r},t) = \hat{H}\Psi_n(\mathbf{r},t) \tag{1.1}$$

where Ψ_n is the n-th quantum mechanical state. The Hamiltonian operator $\hat{H}$ is thus, by definition, the operator which propagates the quantum mechanical system. $\hat{H}$ corresponds to the energy of the system but its form cannot be rigorously derived.[3]

For the calculation of: geometries, electronic energy levels and relative energies of molecules, we can factor out the time dependence of the coordinates of the system (this requires the Hamiltonian to be time independent):

$$\Psi_n(\mathbf{r},t) = \psi_n(t)\Psi_n(\mathbf{r}) \tag{1.2}$$

by inserting eq. (1.2) into eq. (1.1) and rearranging the resulting equation, one can show that the time-dependent and space-dependent parts are separable, and thereby constant (E_n):

$$\hat{H}\Psi_n = E_n\Psi_n \tag{1.3}$$

Solving the eigenvalue eq. (1.3) for E_n gives the energy of the system. In the non-relativistic picture, one can, by relying on the correspondence principle, formulate a Hamiltonian operator compatible with the Hamiltonian in the Lagrangian formulation of classical mechanics. $\hat{H}$ is then given as (still in the absence of time dependent fields):

$$\hat{H} = \hat{T}(\hat{\mathbf{r}}) + \hat{V}(\hat{\mathbf{r}}) \tag{1.4}$$

$$\hat{T} = \frac{\hat{\mathbf{p}}^2}{2m} \tag{1.5}$$

where $\hat{\mathbf{p}} = -i\hbar\nabla$ and $\hat{\mathbf{r}} = \mathbf{r}$. The Hamiltonian is then expressed with contributions of kinetic ($\hat{T}$) and potential ($\hat{V}$) energy.

1.1.2 Many electron systems

The Schrödinger equation can be solved analytically for one-electron systems with fixed nuclei (e.g. the hydrogen atom and the H_2^+ molecule). For larger systems one needs to use numerical methods to solve the eigenvalue equation.

Already during the early days of quantum mechanics considerable progress was made in the formal treatment of the many-body problems, and as PAM Dirac wrote in a paper from 1929:[4]

> "The underlying physical laws necessary for the mathematical theory of a large part of physics and the whole of chemistry are thus completely known, and the difficulty is only that the exact application of these laws leads to equations much too complicated to be soluble."

Dirac is perhaps most known for the Dirac-equation which may be viewed as a Lorentz-covariant form of the Schrödinger equation (the Dirac equation obeys Einstein's theory of special relativity, whereas the Schrödinger equation does not). Relativistic effects are commonly small in chemistry because the electron usually do not approach speeds comparable to the speed of light. However, in order to accurately describe the chemistry and electron spectra of heavy elements, where the large nuclear charge leads to very high expectation values of the momentum of the electron close to the nucleus, one needs to invoke relativistic corrections to the Schrödinger picture.

So far the molecules have been described quantum mechanically, but one knows from experience that the nuclei are heavy enough to be quite accurately described classically. Furthermore, the electron is ~2000 times lighter than the lightest nucleus, the proton, resulting in a much higher average speed for the electrons. The effect of this is a weak coupling between the motions of the nuclei and the electrons. This weak coupling is exploited in the *Born-Oppenheimer* approximation which factors the wave function into an electronic and nuclear part:

$$\Psi_{tot} = \psi_{nucl}\psi_{elec} \tag{1.6}$$

where Ψ_{tot} is a function of the position of both the nuclei and the electrons, ψ_{nucl} is a function of only the nuclei coordinates and ψ_{elec} is a function of the electron coordinates (and parametrically dependent on the nuclear coordinates). Using the Born-Oppenheimer factorization in eq. (1.6), eq. (1.4) can be formulated as a sum of separated nuclear-nuclear, nuclear-electron and electron-electron interaction potentials:

$$\hat{H} = \hat{T}_n + \hat{T}_e + \hat{V}_{nn} + \hat{V}_{ne} + \hat{V}_{nn} \tag{1.7}$$

where n denotes nuclear and e electronic. The use of the Born-Oppenheimer approximation is usually accompanied with the application of the *adiabatic approximation* where the system is restricted to one electronic state. The solution to the Schrödinger equation is then only parametrically dependent on nuclear coordinates, and solving it for different nuclear coordinates, a potential energy surface (PES) may be computed. However, if two such PES corresponding to different electronic states are close to each other with respect to energy for some nuclear configuration, the adiabatic approximation becomes poor. The electronic wave function is then very sensitive to the nuclear coordinates and hence the Born-Oppenheimer approximation breaks down.

1.1.3 Hartree-Fock theory

Since Hartree-Fock (HF) theory and associated electron correlation methods is a large topic, the details of it will not be presented here, but only the central concepts. The interested reader can turn to a textbook for the full theory (*e.g.* ref.[1,5]).

Independent particle model

Central to the HF theory is the independent particle model. It treats each electronic degree of freedom as if it interacts with a *mean field* generated by the other electrons. This implies that HF theory in its simplest form is unable to accurately describe the fact that the movements of the electrons are correlated due to their Coulombic repulsion.

Antisymmetry

One of the axioms of quantum mechanics is the Pauli antisymmetry principle. It demands that a wave function of a many-particle ensemble of fermions is antisymmetric with respect to substitution of any two particles. In practical computations this is usually achieved by using one (HF) or many (multiconfigurational methods) *Slater determinants*:

$$\Psi(\mathbf{x}_1, \mathbf{x}_2, ..., \mathbf{x}_N) = \frac{1}{\sqrt{N!}} \begin{vmatrix} \chi_i(\mathbf{x}_1) & \chi_j(\mathbf{x}_1) & \cdots & \chi_k(\mathbf{x}_1) \\ \chi_i(\mathbf{x}_2) & \chi_j(\mathbf{x}_2) & \cdots & \chi_k(\mathbf{x}_2) \\ \vdots & \vdots & \ddots & \vdots \\ \chi_i(\mathbf{x}_N) & \chi_j(\mathbf{x}_N) & \cdots & \chi_k(\mathbf{x}_N) \end{vmatrix} \tag{1.8}$$

Basis set approximation

In order to conduct numerical computations, the wave function needs to be expanded in a basis set. From the analytic solution of *e.g.* the hydrogen atom, one knows the functional form of the atomic orbitals. However, the functional form of the atomic orbitals include exponential factors, and it turns out that the integration over molecular orbitals in this basis set is numerically expensive. The solution is to use contracted Gaussian functions to approximate the form of the exponential factors. Even though a much larger number of terms is needed, it is computationally more efficient. The notation of basis sets is somewhat esoteric, *e.g.* 6-311+(2df,2p) is to be deciphered as follows: one contracted Gaussian, consisting of six canonical Gaussian functions, is used to represent the core electron orbitals, three contracted Gaussians (one consisting of 3 canonical Gaussians functions, and two consisting of one each) are used to describe the other electrons, the "+" sign signals that an additional diffuse Gaussian is added, and finally the valence electrons have additional polarization functions (hydrogens will have two polarization functions of p-type while other atoms will have two d-type and one f-type polarization functions).

Since one always need to invoke the basis set approximation, one can essentially never compute the "true" energy of any molecule. Fortunately, it turns out that for most systems the energy converges rather quickly with respect to basis set size, and even the extrapolation to the complete basis set limit can be done for small systems if needed.

1.1.4 Electron correlation methods

The error introduced by invoking the independent particle model in HF theory and using a single Slater determinant is not large compared to the total interaction energy (on the order of a percent). Unfortunately, it turns out that a large part of the error is transferred into computed bond dissociation energies when subtracting energies for molecules and fragments. Therefore, it is of crucial importance to use a method which captures as large part of the correlation energy as possible, if one wants to estimate bond strengths and energy barriers.

The deficiency can be treated using *e.g.* explicitly correlated forms of the wave function, multiple Slater determinants or by adding a perturbation to the Hamiltonian operator.

If the Slater determinants are chosen as to include the HF determinant and all the possible determinants which has one electron excited and then all determinants with two electrons excited and so forth, we obtain the truncated *Configuration Interaction* (CI) methods and finally at the limit of all possible excitations: full CI. Full CI is exact within a given basis but it scales as the factorial of the number of basis set functions and it is not possible to use it for anything but the smallest systems.

Perturbative methods is in practice synonymous with Møller-Plesset (MP) methods. MP methods are less expensive than the CI methods while still being able to correct for a large part of the correlation energy.

Coupled Cluster (CC) theory is related to both CI and perturbation theory in the sense that it includes corrections of type (singles, doubles, triples, etc. excitations) to infinite order while MP methods include all types of corrections to a given order. Truncated CC methods are, as opposed to truncated CI, size extensive. In practice the Coupled Cluster method abbreviated CCSD(T) has become the golden standard within the field of electronic structure theory. It treats singles and doubles excitations iteratively and triples excitations perturbatively. The proven accuracy of CCSD(T) motivated its use for single point (no geometry optimization) energy calculations in this work.

1.1.5 Density Functional Theory

The Kohn-Sham formulation[6] of density functional theory (DFT) has become perhaps the most used family of *ab initio* methods in QC. The computational cost is similar to HF, but the performance is superior. In DFT one no longer need to invoke the use of wave functions since the energy of a system is uniquely defined for a given electron density,[7] however, there exists no analytic formulation of the energy in terms of the electron density.

The electron-electron correlation, which is not described by HF, is partly accounted for in DFT. However, the exchange correlation, which arises from the Pauli exclusion principle is lost in the transition from the wave function to the electron density picture. And it is this part of the functional, for which no analytic ex-

pression exists. The consequence is that DFT methods lack a systematic route of improvement.[1] Because of this, more and more heavily parametrized functionals have been developed. One of the most commonly used functionals in chemistry is B3LYP. It uses Becke's three parameter mixing of exchange[8] and the correlation functional of Lee, Yang and Parr.[9] A newer functional which has proven to be superior[10] to B3LYP and many other functionals in predicting bond dissociation energies in N-X species is the M06-2X functional from the M06 functional suite developed in the group of Truhlar.[11] Both B3LYP and M06-2X is used in this work.

1.1.6 Transition state theory

Within the Born-Oppenheimer approximation chemical reactions may be envisaged as rearrangement of the nuclei. Reactants and products of a chemical reaction are local minima on this energy landscape and the path which traverses this landscape in a minimum-energy fashion is called the *reaction path*. During the reaction, the extent of reaction may be formulated in terms of what fraction of the reaction path has been traveled, this metric is commonly called the *reaction coordinate* (ξ). By applying the idea of a quasi equilibrium between reactant and a transition state (TS), one may, for the transient concentration of the TS, formulate the equilibrium constant (for a bi-molecular reaction) as:

$$K_{TS} = \frac{[TS]}{[A][B]} = e^{-\frac{\Delta G^{\ddagger}}{RT}} \tag{1.9}$$

where $[TS]$, $[A]$ and $[B]$ denote the concentration of the transition state, reactant A and reactant B respectively, and ΔG is nothing else than the change in Gibbs free energy, defined as:

$$\Delta G = \Delta H - T\Delta S \tag{1.10}$$

Formally the enthalpy H is

$$\Delta H = \Delta U + P\Delta V \tag{1.11}$$

where U is internal energy, P is the pressure and ΔV is the change in volume. The volume change between reactant and product for the considered reaction is expected to be relatively small (on the order of Å^3), which, assuming ambient conditions, renders the contribution of the $P\Delta V$ term to be on the order of $1 \times 10^{-1}\,\text{kJ mol}^{-1}$.[a] Since the precision of the calculated energy is on the order of $10\,\text{kJ mol}^{-1}$ we can conclude that for all practical purposes we can assume $\Delta U \approx \Delta H$ at ambient conditions.

From the quasi-equilibrium concentration of the TS, the overall rate of reaction can be formulated as (a result of statistical mechanics):

$$k_{reaction} = \kappa \frac{k_B T}{h} K_{TS} \tag{1.12}$$

[a] $P\Delta V \approx 1 \times 10^5\,\text{Pa} \cdot N_A \cdot 1 \times 10^{-30}\,\text{Å}^3 \approx 6 \times 10^{-2}\,\text{J mol}^{-1}$

where κ is the *transmission coefficient*, k_B is Boltzmann's constant, T is the temperature and h is Planck's constant and K_{TS} is the quasi-equilibrium constant of the TS/reactant equilibrium. Assuming the transmission coefficient to be 1 (a common assumption) and after inserting eq. (1.9) into eq. (1.12) one obtains:

$$k_{reaction} = \frac{k_B T}{h} e^{-\frac{\Delta G^{\ddagger}}{RT}} \tag{1.13}$$

For light elements, such as hydrogen this estimate might not be accurate due to tunneling effects. However, for the tunneling correction to be made, one would like at least comparable accuracy in the barrier heights effect, as in the tunneling effect. The next step is to calculate entropy change, ΔS. From statistical mechanics we can express the entropy of the system in the canonical ensemble from the partition function Q:

$$S = k_B T \left(\frac{\partial \ln Q}{\partial T} \right)_V + k_B \ln Q \tag{1.14}$$

For an isolated di- or triatomic system one can analytically express the partition function Q within the rigid-rotor-harmonic-oscillator (RRHO) approximation.[1] And for a system of non-interacting particles, the partition function of the system can be decomposed into the contribution of the individual molecular partition functions q_i for different molecules of kind i with a population N_i:

$$Q = \frac{\prod_i q_i^{N_i}}{\prod_i N_i!} \tag{1.15}$$

The RRHO approximation allows one to formulate the molecular partition function as a product of translational, rotational, vibrational and electronic contributions (in the absence of an external magnetic field):

$$q = q_{trans} q_{rot} q_{vib} q_{elec} \tag{1.16}$$

This factorization assumes good separability between these contributions, which is the case for the majority of systems. However, rovibrational coupling, as well as electronic-vibrational coupling, sometimes render this simplification too crude. In that case, those contributions cannot be calculated independently. Applying eqs. (1.15) and (1.16) to eq. (1.14) one can write:

$$S_{tot} = S_{trans} + S_{rot} + S_{vib} + S_{elec} \tag{1.17}$$

In the condensed phase both the approximation of decomposition of the system's partition function, Q, into molecular partition functions, q, as well as the factorization of the molecular partition function, are no longer good approximations. And even if the factorization is made, rotation and translation of molecules are now hindered. Hence, in the condensed phase, one can no longer find an analytic formula for the partition function. In order to obtain an accurate description of such systems, one needs to formulate the interaction energy in closed form and sample

the phase space. The size of the system often make *ab initio* methods too costly, limiting the choice to more parametrized descriptions. The proper sampling of the phase space can be achieved by simulating the evolution of the system using either molecular dynamics or Monte Carlo procedures, where the interaction of the atoms are described by a parametrized force-field.

1.1.7 Sampling techniques

In order to have a better estimate of the entropy contribution, molecular dynamics or Monte Carlo methods could be used, however, it is not trivial how to treat the transaction between the picture of quantum and classical mechanics.

If one resorts to a non-reactive force field based method in the sampling of the phase space connected to a reaction, one needs a way to connect the probability of reaching the transition state with the overall rate constant. A common way, is to reduce the degrees of freedom in the analysis of the trajectories from *e.g.* MD simulations, and employ the idea of a *near attack coordinate*. The near attack coordinate is then formulated as one or a couple of physically relevant metrics, *i.e.*the distance between two reacting species. However, such treatment is outside the scope of this work.

1.1.8 This work

The relative energy between several conformations of reactants, transition states and products of reacting species in aqueous solution have been calculated by *ab initio* methods. The phase space has been manually explored with respect to solute structuring around the reacting species in order to make a survey of the energy landscape (with vibrational corrections to partly include entropic effects).

The usual way of treating solvation effects in QM computations is to use a polarizable continuum model. And in the case of reactions where the solute is directly involved in the reaction, these are added in a minimum number fashion.[12]

The convergence and agreement with experiment with respect to the number of included water molecules is investigated for both the reaction barriers as well as the absorption spectrum of $H_2NOO^{\bullet}$. However, as the number of explicit water molecules in the model increase, so does the workload of the manual exploration, in fact, the work grows exponentially.

The manual exploration does raise the question whether the potential (free) energy surface is sufficiently sampled and for an even larger number of water molecules one really needs to resort to QM/MM or MD to make an accurate approximation of the entropy part of the free energy reaction barriers. But the automation comes at a cost, a much larger number of conformations needs to be sampled and hence the higher levels of theory are no longer available.

A first approximation of the entropy contributions to the free energy can be made by approximating:

$$\Delta S_r \approx \Delta S_{vib} \tag{1.18}$$

since the energy of other electronic potential energy surfaces was not found to lie close in the studied system, negligible contribution is expected to the partition function from electronically excited states and hence the S_{elec} term from eq. (1.17) cancel when calculating ΔS_{elec}. ΔS_{rot} and ΔS_{trans} are expected to give a negligible (maybe also spurious) contribution to the reaction barrier, and are therefore not included in its computation.

In order to calculate S_{vib} we utilize the analytic expression of the vibrational part of the molecular partition function (within the harmonic oscillator approximation):

$$q_{vib} = \prod_{i=1}^{3N_{atom}-6(7)} \frac{e^{-h\nu_i/2k_BT}}{1-e^{-h\nu_i/k_BT}} \tag{1.19}$$

where ν_i is the i: th vibrational frequency, and 7 degrees of freedom is subtracted instead of 6 in the case of a TS. By inserting eq. (1.19) into eq. (1.14) one obtains:

$$S_{vib} = k_B \sum_{i=1}^{3N_{atom}-6(7)} \left(\frac{h\nu_i}{kT} \frac{e^{-h\nu_i/k_BT}}{1-e^{-h\nu_i/k_BT}} - \ln\left(1-e^{-h\nu_i/k_BT}\right) \right) \tag{1.20}$$

This will serve as a approximation of the entropy when calculating Gibbs free energy. The tunneling contribution to the rate constant has not been considered due to reasons discussed above.

1.2 Radiation chemistry

Radiation chemistry is the field which studies chemical reactions induced by ionizing radiation. In this work we are exclusively interested in the aqueous phase radical oxidation of ammonia, and radiation chemistry will provide us with the tools needed to investigate the radical reactions leading to the final oxidation. In order to make this report more self-contained, the central basics of the *water radiolysis* and radiation's interaction with matter, is presented in this section.

1.2.1 Radiation-matter interaction

When ionizing radiation interacts with liquid water, several processes occur, which eventually lead to the formation of a number of radical and molecular species. The yields of these species depend on what kind of radiation is deposited in the liquid. In this work, γ-radiation, which has a large penetration depth, was employed. Because of this, the γ-field intensity can accurately be assumed to be constant throughout the sample. One should not be fooled to believe that the *energy deposition* is homogeneous. The γ-rays have a very low probability of interacting with the water molecules (the cross-section is low), but once interacting the energy deposited is very large compared to chemical bonds. A single γ-ray can cause tens of thousands of chemical events from secondary photons and particles. The interaction of γ-rays with water (or any matter) can be divided into:

Coherent scattering
: When γ-rays are coherently scattered, the energy of the photon remains essentially unchanged and no considerable amount of energy is deposited in the material.

Compton scattering
: The Compton effect is the scattering interaction between a γ-ray and an electron. In Compton scattering the photon is deflected with a lower energy and the energy difference is transferred to the electron in the form of kinetic energy.

Photoelectric effect
: When a γ-ray is absorbed by the photoelectric effect all energy of the photon is deposited in the material and a bound orbital electron is then ejected with (in chemical terms) very high kinetic energy. If a core electron was ejected, X-rays and Auger electrons will be emitted as the vacancy is repopulated with electrons from higher shells.

Pair production
: Pair production is the conversion of a γ-photon into an electron and a positron. The process occurs at the nucleus of an atom and the probability increases with the atom number of the nucleus and the energy of the γ-photon. Since the rest mass of the electron (and the positron) is 0.51 MeV, the process requires

Specie	Yield[15] / 10^{-7} mol Gy^{-1}
H_2O	−4.81
e^-_{aq}	2.69
$\dot{H}$	0.68
H_2	0.47
$\dot{O}H$	2.80
H_2O_2	0.73
$H\dot{O}_2$	0.02
H^+	3.21
OH^-	0.52

Table 1.1: Primary yields of aqueous γ-radiolysis

a γ-photon with a minimum energy of 1.02 MeV. Any excess energy of the photon is converted into kinetic energy of the formed pair.

The main mode of interaction of γ rays of an energy of about 0.1 MeV to 10 MeV with water is the Compton effect.[13] The ionizing radiation's interaction with the water leave tracks within the liquid made by secondary energy carriers (secondary electrons and X-rays in the case of γ radiation) originating at the point of the primary interaction. This is known as *spur formation* and happens during what is called the *physical stage* of the interaction. Approximately 10^{-7} s after the initial primary interaction, diffusion processes have rendered the solution homogeneous and we are left with the long lived molecular products and the radical species with intermediate lifetime.[14] The yield of these species depend on what kind of radiation is applied. For γ-radiolysis the primary radiolytic yields are presented in table 1.1.

1.2.2 Caesium-137

In this work a ^{137}Cs γ-source was employed. ^{137}Cs has a lifetime of 30.07 years and decays to ^{137m}Ba by β^--decay. With 94.4% probability, the daughter nuclide is in the meta stable state, and there is a 5.6 % probability that it decays directly to the ground state of ^{137}Ba. ^{137m}Ba has a lifetime of 2.552 min (and decays to ^{137}Ba) and emits a γ-photon with an energy of 662 keV.[16] The details of the energies and decay rates are not very important in the practical application to radiation chemistry because the dose rate of the γ-cell is determined using dosimetry which is explained in section 1.2.3. But we can note that the half-life of ^{137}Cs is very long in comparison to the time scales of the experiments in this work.

1.2.3 Dosimetry

When irradiating a material in a scientific study, knowledge of how much energy has been deposited in the material (*i.e.* the dose, denoted D) is crucial. The dose is measured as energy deposited per unit mass of material and it is expressed within the SI-unit system as the compound unit "Gray" (Gy) which is equal to $\mathrm{J\,kg^{-1}}$.

Since the ^{137}Cs γ-source can be viewed as having a constant (*cf.* section 1.2.2) dose rate ($\dot{D}$) during the irradiation, we only need to determine the dose rate of the γ-source. This was done in this work using the Fricke dosimeter[13] which is based on the oxidation of $Fe^{2+}$to Fe^{3+}in acidic oxygenated aqueous solution. The yield of Fe^{3+}, $G(Fe^{3+})$, can easily be determined spectroscopically using a UV/vis spectrophotometer. By comparing the observed production rate with the known yields reported in the literature the dose rate is calculated as:

$$G(Fe^{3+}) = 2 \cdot G(H_2O_2) + 3 \cdot \left(G(e^-_{aq}) + G(^{\bullet}H) + G(\ HO^{\bullet}_2)\right) + G(^{\bullet}OH) \tag{1.21}$$

$$\dot{D} = \frac{A}{\epsilon b \rho G(Fe^{3+})} \tag{1.22}$$

where A is the absorbance, ϵ is the extinction coefficient ($217.4\,\mathrm{m^2\,mol^{-1}}$) of Fe^{3+}at the used wavelength (304 nm), b is the cuvette length, ρ is the density of the solution ($1024\,\mathrm{kg\,m^{-3}}$). $G(Fe^{3+})$ is known via eq. (1.21) and table 1.1 to be $1.443 \times 10^{-6}\,\mathrm{mol\,J^{-1}}$.

1.2.4 Competition kinetics

The method of determining relative reaction rates between two competing reactions can be done by employing *competition kinetics*. In this work, the concept was applied to the two reactions:

$$^{\bullet}OH + NH_3 \longrightarrow {}^{\bullet}NH_2 + H_2O \tag{1.23}$$

$$^{\bullet}OH + OH^- \longrightarrow {}^{\bullet}O^- + H_2O \tag{1.24}$$

here we are assuming that the fate of $^{\bullet}OH$ is determined by the two competing reactions 1.23 and 1.24. If the yield of our final product depend on $^{\bullet}NH_2$ as its limiting reactant, and if there is no pathway from $^{\bullet}O^-$ leading to the product, then the observed yield should be directly proportional to the branching ratio of reaction 1.23. Let us call the branching ratio (or relative yield) Q, then we can formulate it in terms of $[NH_3]$ as:

$$Q = \frac{k_{1.23}[^{\bullet}OH][NH_3]}{k_{1.23}[^{\bullet}OH][NH_3] + k_{1.24}[^{\bullet}OH][OH^-]} \tag{1.25}$$

$$\tag{1.26}$$

If these assumptions are good we see that from reformulating eq. (1.26) to eq. (1.27) we would expect a linear relationship between the reciprocal relative yield and the reciprocal concentration of NH_3:

$$\frac{1}{Q} = 1 + \frac{k_{1.24}[OH^-]}{k_{1.23}} \frac{1}{[NH_3]} \tag{1.27}$$

From table 2.1 we can see that the assumption of $\dot{O}^-$ not leading to product will not be valid, its reaction with $NH_3$is only a factor 3 lower than $\dot{O}H$ but the principle behind the technique is nicely illustrated above.

1.3 Modeling of systems of reactions

The fundamental reactions of water radiolysis is well known and the most important species are well characterized. Using the vast quantitative kinetic data, large models can be made, consisting of the elementary reactions involved, together with their respective rate constants.

1.3.1 Transformation to a system of equations

From the law of mass action and the elementary reactions, coupled equations governing the time evolution of the concentrations can be formulated. Together they form a first order autonomous non-linear system of ordinary differential equations:

$$\frac{dC_i}{dt} = \sum_j r_j S_{ij} \tag{1.28}$$

$$r_j = k_j \prod_k C_k^{R_{kj}} \tag{1.29}$$

where S_{ij} is the net stoichiometric change of the species i in reaction j, r_j is the reaction rate of reaction j, and is according to the law of mass action proportional to the concentration of each reactant C_k to the power of its stoichiometric coefficient as a reactant, R_{jk}.

The homogeneous kinetics of the radiolytic oxidation of ammonia to peroxynitrite was simulated using a custom software written specifically for the project. The available software for simulating kinetics of radiochemical processes e.g. MAKSIMA CHEMIST lacks the flexibility of modern more general purpose (bio)chemical simulation software such as COPASI. When systems of interest were solved using COPASI numerical instability occurred using the supplied deterministic solver LSODA.[17] Therefore a modern meta-programming approach was chosen to rapidly develop a software framework, PyKinetics (*cf.* sections 1.5 and 3.5 in the supplementary material), for the analysis of radiochemical processes. The framework is written in the dynamically and strongly-typed language Python. The use of a dynamic language give well recognized advantages in development time. However, the numerical integration of large systems became too slow (or even failed) when compared to statically typed, compiled programming languages such as C or Fortran. In order to remedy this deficiency, the symbolically derived algebraic expressions for the ODE equations and the corresponding Jacobian, were exported to Cython[b] code on the fly. The symbolic algebraic treatment was done by leveraging the SymPy package[c]. The code generator was designed to generate functions with the correct signature for use with the GNU Scientific Library[d] (GSL). The stepper used was the semi-implicit Bürlish-Stoer method of Bader and Deufelhard.[18] In summary the control flow of the program is as follows:

[b] Available at http://www.cython.org
[c] Available at http://www.sympy.org
[d] Available at www.gnu.org/s/gsl/

1. Generation of algebraic expressions for the ODE system.
2. Symbolic derivation of Jacobian.
3. GSL compatible Cython code generation.
4. Compilation to machine code.
5. Integration with user specified parameters.
6. Generation of time series data and plots.

The time of integration was improved by approximately a factor of 40 in comparison to the pure python version. Now, however, the integration is no longer the time determining step but rather step 4 above.

1.3.2 Comparison with experiment

In the experiments, before irradiation, the samples were at equilibrium. The initial concentrations in the simulation should therefore be compatible with all chemical equilibria in the system. In order to ease the input of data for all simulations corresponding to experimental data points (which often had slightly different initial concentrations), a routine to solve the system of non-linear equations of the coupled chemical equilibria was written. The reason for not using available software such as Medusa was the need for a scriptable interface, the manual computation of hundreds of equilibrium concentrations is error prone and late revisions are very labor intensive.

To solve the system of equations resulting from generic reaction systems, one needs in addition to the equilibrium constants, additional relations to ensure to have at least the same number of relations as unknowns. Since initial (non-equilibrium concentrations) are known, one can either deduce additional boundary conditions or solve not for the concentrations, but for the extent of each reaction. The latter approach however, gave rise to numerically ill-conditioned systems, and initial experiments showed that the method failed for any system more complex than trivial examples. The conclusion was that this formulation was not suited for a robust numerical routine. Instead the system was solved for all concentrations, and employing the conservation of mass and charge to formulate a, sometimes overdetermined, system. This system was then solved for the logarithm of the concentrations using the Levenberg-Marquardt algorithm[19] as implemented in MINPACK[20] and conveniently wrapped in SciPy[e].

The equilibrium constant K of a chemical equilibrium is defined as:

$$K_j = \prod_k C_j'^{S_{kj}} \tag{1.30}$$

[e] Available at http://www.scipy.org

where, as in the case of the kinetic expressions, S_{kj} is the net stoichiometric coefficient of species k in reaction j. Here C'_j is the concentration at *equilibrium* whereas using the transient concentration:

$$Q_j = \prod_k C_j^{S_{kj}} \tag{1.31}$$

one obtains the conventional quantity Q, known as the *reaction quotient*. The equations to be solved for, corresponding to the chemical equilibria were chosen to be expressed as:

$$y_i = \ln K_i - \ln Q_i \tag{1.32}$$

Where $\ln Q_i$ is a function of $\ln C_j$ for all species j in equilibrium i. The details of the implementations can be seen in the source code (*cf.* section 3.5.18 in supplementary material).

Chapter 2

Present Investigation

This chapter contains the introduction to the scientific problem studied, the description of the methods used, the results and finally the conclusions made from the work.

2.1 Introduction

Ammonia is both a naturally occurring and widely used chemical, both in industry and agriculture. Although it is very soluble in water, its low boiling point (-33° C) make it an considerable air pollutant. The gas-phase free radical reaction between ammonia-derived radicals and oxygen-containing species are the main mode of photolytic ammonia oxidation in the troposphere and the lower parts of the stratosphere.[21,22] The oxidation generates nitrogen oxides, and hence insight in the mechanism of ammonia oxidation is of great importance in order to make accurate assessments of the environmental impact of anthropogenic ammonia released into the atmosphere. Fundamental knowledge on the radical reactions of ammonia-derived species is also important in biochemistry, since the oxidation products are known to be cytotoxic.[23,24] Furthermore, one of the considered fuels for future generation IV nuclear reactors is uranium nitride.[25] The safety assessment of future nuclear reactors and nuclear fuel deep repositories will then need very detailed understanding of elementary radical reactions of nitrogen species in water radiolysis. The reason for this is that the hydrolysis of uranium nitride form ammonia.[26]

In this work, the reactions of the aminyl radical ($\cdot NH_2$, also known as amidogen radical) with molecular oxygen (*cf.* eq. (2.1)) and the superoxide anion (*cf.* eq. (2.2)) are studied both experimentally (using γ-radiolysis) and theoretically (using ab initio quantum chemical methods at different levels of theory). The two reactions can be summarized as:

$$\cdot NH_2 + O_2 \longrightarrow Products \tag{2.1}$$

$$\cdot NH_2 + O_2^{-\cdot} \longrightarrow Products \tag{2.2}$$

The reactions of the aminyl radical with molecular oxygen in the gas-phase has been the subject of many experimental studies[27–29] as well as theoretical investigations.[30,31]

The reaction of $^{\bullet}NH_2$ with O_2 in the aqueous phase has also been studied experimentally.[32–39] But the suggested mechanism in ref.[32] for water-mediated hydrogen shifts has not, to the author's knowledge, been studied theoretically. The suggested mechanism is presented in fig. 2.1. The reaction is expected to proceed via two transition states (*cf.* figs. 2.2 and 2.3). The reaction between $^{\bullet}NH_2$ and O_2 has a much larger observed reaction rate in aqueous solution[32,33] in comparison to gas-phase. One of the aims of the theoretical calculations is to show whether or not the transition states of those in figs. 2.2 and 2.3 can explain the increased rate of reaction in water. The second use is the benchmarking of the theoretical treatment against the available experimental kinetic data. Agreement between theory and experiment for those reactions with reported rates strengthen the purely theoretical estimates of those for which no experimental data exists.

The species measured was the peroxynitrite anion, $ONOO^-$. The change in its production in aqueous γ-radiolysis of ammonia for systems with different ratios of primary production of $^{\bullet}OH$ and $^{\bullet}O_2^-$ was investigated. The ratio between these primary radicals was adjusted by varying the ratio of N_2O and O_2 in the samples, something which does not seem to have been done earlier. It is expected that $ONOO^-$ is primarily formed via reaction 141 in table 2.1 where the main path to NO is expected to be from reaction 165 via reaction 95. Applying this simplified scheme to the reaction conditions in the experiments would suggest that either $^{\bullet}OH$ or $^{\bullet}O_2^-$ can be the limiting reactant, both having a stoichiometric ratio of 1:1 to formed $ONOO^-$.

Both N_2O and O_2 compete in the reaction with e_{aq}^- and $^{\bullet}H$ (*cf.* reaction 29,43,121 and 121 in table 2.1). These two processes are the dominant source of the altering of the ratio of $^{\bullet}OH/^{\bullet}O_2^-$. Formulating the effective radiolytic yields in terms of these reactions gives:

$$G_{tot}(^{\bullet}O_2^-) = G_i(^{\bullet}O_2^-) + G_i(e_{aq}^-)\frac{r_{29}}{r_{121}+r_{29}} + G_i(^{\bullet}H)\frac{r_{43}}{r_{122}+r_{43}} \tag{2.3}$$

$$G_{tot}(^{\bullet}OH) = G_i(^{\bullet}OH) + G_i(e_{aq}^-)\frac{r_{121}}{r_{121}+r_{29}} + G_i(^{\bullet}H)\frac{r_{122}}{r_{122}+r_{43}} \tag{2.4}$$

Also the gas-phase reaction between the aminyl radical and the superoxide anion ($^{\bullet}O_2^-$) radical, and the related reaction between the imine radical ($\cdot\underline{\dot{N}}H$) and hydroperoxyl radical ($\cdot OH_2$), have been studied theoretically.[31,40] Also here, no theoretical study incorporating explicit solvent water, which might lower hydrogen shift transition states, have been found. Therefore the same theoretical treatment is performed for the former of those reactions. The proposed reaction mechanism (*cf.* fig. 2.4) of a hydrogen shift from N to terminal O is presented in fig. 2.4. It should be noted that the product of the consecutive step, which is expected to be the nitroxyl anion, could be both in a singlet or triplet state. Energetically, the triplet state is known to be more stable.[41]

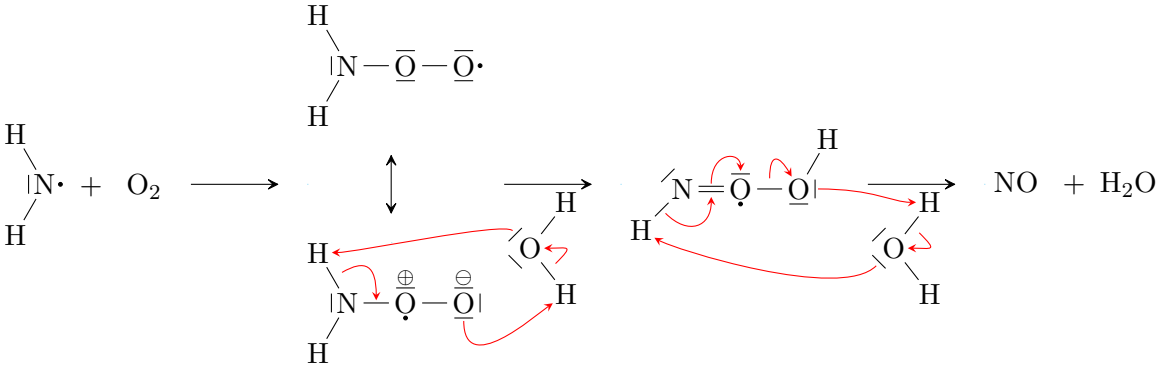

Figure 2.1: Mechanism evaluated using ab initio methods for the reaction between aminyl radical and molecular oxygen in aqueous solution.

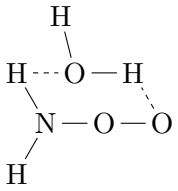

Figure 2.2: TS of $NH_2OO^{\bullet} \rightarrow NHOOH$

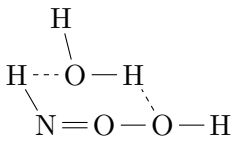

Figure 2.3: TS of $^{\bullet}NHOOH \rightarrow NO^{\bullet} + H_2O$

The γ-radiolysis experiments are combined with the modeling of the reaction system by using a compiled list of reactions from the literature thought to have importance in the radiolysis (*cf.* table 2.1). One way of gaining insight to what parts of the model that are better described than others, is to evaluate the accuracy of simple competition kinetics models in relation both to the model and to the experiment.

2.2 Experimental and computational methods

2.2.1 Instrumentation

The γ-radiolysis experiments were performed using an MDS Nordion 1000 Elite Cs-137 γ-source with dose rates varying by irradiation position from 0.1 to 0.3 Gy s^{-1}. The dose rate was determined using Fricke dosimetry.[13] The concentration

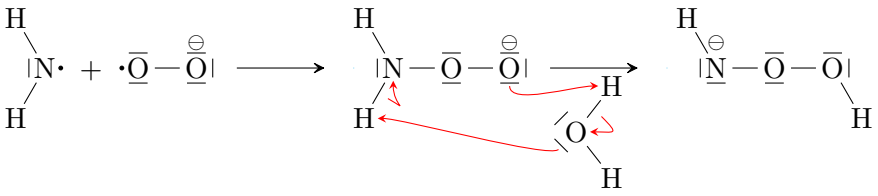

Figure 2.4: Mechanism evaluated using ab initio methods for the reaction between aminyl radical and superoxide anion in aqueous solution.

of formed $ONOO^-$ was monitored by UV/vis spectroscopy at 302 nm using an extinction coefficient of 167 $m^2\,mol^{-1}$.[42]

2.2.2 Reagents and experiments

Millipore Milli-Q water was used for the preparation of all solutions. The aqueous ammonia used for the preparation of the solutions was from Sigma-Aldrich (p.a.). The NaOH (p.a.) used was bought from Merck. The gas mixtures used for saturation of the aqueous solutions were 80/20, 50/50 and 0/100 mole-% N_2O/O_2 respectively. All gases were bought from AGA.

The solutions were prepared (*cf.* fig. 2.5) by adding 5 ml of gas saturated water to 20 ml glass vials. The vials were then flushed with the same gas mixture for ten minutes. Finally, the pH was adjusted by adding concentrated solutions of NaOH and NH_3(together making a contribution of less than 10% to the total volume). The samples were then sealed with multiple layers of polymer film and exposed to one continuous γ-irradiation of known time and dose rate. The effective radiolytic yields of $ONOO^-$ (G_{ONOO^-}) were determined from irradiation time scans for each of the atmospheres. The expected effective yields were calculated according to the competition kinetics eqs. (2.3) and (2.4).

2.2.3 Modeling

The modeling of the radiolysis of the aqueous ammonia solutions was done using a custom software[43] for the integration of the first-order autonomous ODE system. The reactions included in the model are presented in table 2.1.

Table 2.1: Reaction used for modeling aqueous radiolysis of ammonia. The rate constants are valid for $[H_2O] = 1.0$ M. The unit of the rate constants depends on the number of reactants associated with it, n, and is expressed as: $M^{1-n} \cdot s^{-1}$. The exception is reaction 1–6, (rate constants preceded by a "γ :"). For these six reactions, the number listed is the radiolytic yield (primary production) for γ-radiolysis of water, and has the unit $mol\,J^{-1}$.

Id.	Reactants		Products		Rate constant	Ref
1	H_2O	$\rightarrow$	$H^+ + OH^-$	γ:	5.18×10^{-8}	[15]

Table 2.1: continued

Id.	Reactants		Products		Rate constant	Ref
2	H_2O	→	$e^-(aq) + H^+ + OH\cdot$	γ:	2.69×10^{-7}	15
3	H_2O	→	$H\cdot + H_2O_2$	γ:	6.84×10^{-8}	15
4	H_2O	→	$H_2 + H_2O_2$	γ:	7.67×10^{-8}	15
5	H_2O	→	$H_2 + OH\cdot$	γ:	1.04×10^{-8}	15
6	H_2O	→	$H_2 + HO_2$	γ:	4.15×10^{-9}	15
7	$H^+ + OH^-$	→	H_2O		1.4×10^{11}	44
8	H_2O	→	$H^+ + OH^-$		0.0014	44
9	H_2O_2	→	$H^+ + HO_2^-$		0.112	45
10	$H^+ + HO_2^-$	→	H_2O_2		5×10^{10}	46
11	$OH^- + H_2O_2$	→	$H_2O + HO_2^-$		1.3×10^{10}	15
12	$H_2O + HO_2^-$	→	$OH^- + H_2O_2$		5.82×10^{7}	$k_{bw} \cdot K_w$ / $K_a(H_2O_2)$
13	$e^-(aq) + H_2O$	→	$H\cdot + OH^-$		19	47
14	$H\cdot + OH^-$	→	$e^-(aq) + H_2O$		2.2×10^{7}	47
15	$H\cdot$	→	$e^-(aq) + H^+$		3.91	$k_{fw} \cdot K_a(H^\bullet)$
16	$e^-(aq) + H^+$	→	$H\cdot$		2.3×10^{10}	47
17	$OH^- + OH\cdot$	→	$O^- + H_2O$		1.3×10^{10}	47
18	$O^- + H_2O$	→	$OH^- + OH\cdot$		1.04×10^{8}	$k_{bw} \cdot K_w$ / $K_a(^\bullet OH)$
19	$OH\cdot$	→	$H^+ + O^-$		0.126	$k_{bw} \cdot K_a(^\bullet OH)$
20	$H^+ + O^-$	→	$OH\cdot$		1×10^{11}	15
21	HO_2	→	$H^+ + O_2^-$		1.35×10^{6}	$k_{bw} \cdot K_a(^\bullet HO_2)$
22	$H^+ + O_2^-$	→	HO_2		5×10^{10}	15
23	$OH^- + HO_2$	→	$H_2O + O_2^-$		5×10^{10}	15
24	$H_2O + O_2^-$	→	$OH^- + HO_2$		18.6	$k_{bw} \cdot K_w$ / $K_a(HO_2^\bullet)$
25	$e^-(aq) + OH\cdot$	→	OH^-		3×10^{10}	47
26	$e^-(aq) + H_2O_2$	→	$OH^- + OH\cdot$		1.4×10^{10}	47
27	$e^-(aq) + H_2O + O_2^-$	→	$OH^- + HO_2^-$		1.3×10^{10}	47
28	$e^-(aq) + HO_2$	→	HO_2^-		2×10^{10}	47
29	$e^-(aq) + O_2$	→	O_2^-		2.22×10^{10}	15
30	$2e^-(aq) + 2H_2O$	→	$H_2 + 2OH^-$		5.5×10^{9}	48
31	$e^-(aq) + H\cdot + H_2O$	→	$H_2 + OH^-$		2.5×10^{10}	47
32	$e^-(aq) + HO_2^-$	→	$OH^- + O^-$		3.5×10^{9}	47
33	$e^-(aq) + O^- + H_2O$	→	$2OH^-$		2.2×10^{10}	47
34	$e^-(aq) + H_2O + O_3^-$	→	$2OH^- + O_2$		1.6×10^{10}	47
35	$e^-(aq) + O_3$	→	O_3^-		3.6×10^{10}	15
36	$H\cdot + H_2O$	→	$H_2 + OH\cdot$		11	47
37	$H\cdot + O^-$	→	OH^-		1×10^{10}	47
38	$H\cdot + HO_2^-$	→	$OH^- + OH\cdot$		9×10^{7}	15
39	$H\cdot + O_3^-$	→	$OH^- + O_2$		1×10^{10}	15
40	$2H\cdot$	→	H_2		7.75×10^{9}	15
41	$H\cdot + OH\cdot$	→	H_2O		7×10^{9}	47
42	$H\cdot + H_2O_2$	→	$H_2O + OH\cdot$		9×10^{7}	47
43	$H\cdot + O_2$	→	HO_2		2.1×10^{10}	47
44	$H\cdot + HO_2$	→	H_2O_2		1×10^{10}	47
45	$H\cdot + O_2^-$	→	HO_2^-		2×10^{10}	48
46	$H\cdot + O_3$	→	HO_3		3.8×10^{10}	48
47	$2OH\cdot$	→	H_2O_2		3.6×10^{9}	47
48	$HO_2 + OH\cdot$	→	$H_2O + O_2$		6×10^{9}	49
49	$O_2^- + OH\cdot$	→	$OH^- + O_2$		8.2×10^{9}	47
50	$H_2 + OH\cdot$	→	$H\cdot + H_2O$		4.3×10^{7}	47
51	$H_2O_2 + OH\cdot$	→	$H_2O + HO_2$		2.7×10^{7}	47
52	$O^- + OH\cdot$	→	HO_2^-		2×10^{10}	47
53	$HO_2^- + OH\cdot$	→	$OH^- + HO_2$		7.5×10^{9}	48
54	$O_3^- + OH\cdot$	→	$OH^- + O_3$		2.55×10^{9}	47
55	$O_3^- + OH\cdot$	→	$H^+ + 2O_2^-$		5.95×10^{9}	47
56	$O_3 + OH\cdot$	→	$HO_2 + O_2$		1.1×10^{8}	47
57	$O_2^- + HO_2$	→	$HO_2^- + O_2$		8×10^{7}	47
58	$2HO_2$	→	$H_2O_2 + O_2$		7×10^{5}	46
59	$O^- + HO_2$	→	$OH^- + O_2$		6×10^{9}	46
60	$HO_2 + H_2O_2$	→	$H_2O + O_2 + OH\cdot$		0.5	15
61	$HO_2 + HO_2^-$	→	$OH^- + O_2 + OH\cdot$		0.5	46
62	$HO_2 + O_3^-$	→	$OH^- + 2O_2$		6×10^{9}	15
63	$HO_2 + O_3$	→	$HO_3 + O_2$		5×10^{8}	15

Table 2.1: continued

Id.	Reactants		Products	Rate constant	Ref
64	$2H_2O + 2O_2^-$	→	$2OH^- + H_2O_2 + O_2$	100	[15]
65	$O^- + O_2^- + H_2O$	→	$2OH^- + O_2$	6×10^8	[47]
66	$O_2^- + H_2O_2$	→	$OH^- + O_2 + OH\cdot$	0.13	[46]
67	$O_2^- + HO_2^-$	→	$OH^- + O^- + O_2$	0.13	[15]
68	$H_2O + O_2^- + O_3^-$	→	$2OH^- + 2O_2$	1×10^4	[50]
69	$O_2^- + O_3$	→	$O_3^- + O_2$	1.5×10^9	[46]
70	$2O^- + H_2O$	→	$OH^- + HO_2^-$	1×10^9	[47]
71	$O^- + O_2$	→	O_3^-	3.6×10^9	[47]
72	$H_2 + O^-$	→	$H\cdot + OH^-$	8×10^7	[47]
73	$O^- + H_2O_2$	→	$H_2O + O_2^-$	5×10^8	[47]
74	$O^- + HO_2^-$	→	$OH^- + O_2^-$	4×10^8	[47]
75	$O^- + O_3^-$	→	$2O_2^-$	7×10^8	[50]
76	$O^- + O_3$	→	$O_2^- + O_2$	5×10^9	[15]
77	O_3^-	→	$O^- + O_2$	300	[51]
78	$H^+ + O_3^-$	→	$O_2 + OH\cdot$	9×10^{10}	[52]
79	$O_3^- + H_2O_2$	→	$H_2O + O_2^- + O_2$	1.6×10^6	[51]
80	$O_3^- + HO_2^-$	→	$OH^- + O_2^- + O_2$	8.9×10^5	[51]
81	$H_2 + O_3^-$	→	$H\cdot + O_2 + OH^-$	2.5×10^5	[51]
82	HO_3	→	$O_2 + OH\cdot$	1.1×10^5	[53]
83	$HO_3 + OH\cdot$	→	$H_2O_2 + O_2$	5×10^9	[54]
84	$2HO_3$	→	$H_2O_2 + 2O_2$	5×10^9	[54]
85	$O_2^- + HO_3$	→	$OH^- + 2O_2$	1×10^{10}	[54]
86	HO_3	→	$H^+ + O_3^-$	328	[53]
87	$H^+ + O_3^-$	→	HO_3	5.2×10^{10}	[53]
88	$OH^- + O_3$	→	$O_2^- + HO_2$	70	[55]
89	$O_3 + HO_2^-$	→	$O_2^- + O_2 + OH\cdot$	2.8×10^6	[55]
90	$2\cdot NH_2$	→	H_2NNH_2	2.2×10^9	[56]
91	$H_2O_2 + \cdot NH_2$	→	$H_2O + \cdot NHOH$	9×10^7	[56]
92	$OH^- + \cdot NHOH$	→	$H_2O + \cdot NHO^-$	1×10^{10}	[57]
93	$H_2O + \cdot NHO^-$	→	$OH^- + \cdot NHOH$	1×10^8	[57]
94	$\cdot NHO^- + O_2$	→	$O_2^- + HNO$	2.2×10^8	[57]
95	$O_2 + \cdot NH_2$	→	$\cdot NH_2O_2$	1.1×10^9	[33]
96	$\cdot NH_2 + OH\cdot$	→	NH_2OH	9.5×10^9	[56]
97	$O_3 + NH_3$	→	Unk.	20	[58]
98	$NH_3 + OH\cdot$	→	$H_2O + \cdot NH_2$	9.9×10^7	[59]
99	$O^- + NH_3$	→	$OH^- + \cdot NH_2$	3×10^7	[60]
100	$H\cdot + NH_3$	→	$e^-(aq) + NH_4^+$	6.7×10^5	[61]
101	$O_3^- + NH_3$	→	$OH^- + \cdot NH_2O_2$	1.7×10^4	[34]
102	$O_3^- + \cdot NH_2$	→	$O^- + \cdot NH_2O_2$	1×10^9	Assumption
103	$e^-(aq) + NH_4^+$	→	$H\cdot + NH_3$	1.7×10^4	[61]
104	$O_3 + NH_2OH$	→	Unk.	2.1×10^4	[58]
105	$O_3 + NH_3OH^+$	→	Unk.	1.7×10^4	[58]
106	$e^-(aq) + NO_3^-$	→	NO_3^{2-}	9.7×10^9	[62]
107	$NO_3^{2-} + H_2O$	→	$2OH^- + \cdot NO_2$	5.5×10^4	[63]
108	$e^-(aq) + NH_2OH$	→	$OH^- + \cdot NH_2$	9.2×10^8	[64]
109	$e^-(aq) + NH_3OH^+$	→	$NH_3 + OH\cdot$	1.2×10^{10}	[64]
110	$NH_2OH + OH\cdot$	→	$H_2O + \cdot NHOH$	9.5×10^9	[64]
111	$NH_3OH^+ + OH\cdot$	→	$H_2O + \cdot NH_2 + OH\cdot$	5×10^8	[64]
112	$e^-(aq) + H_2NNH_2$	→	Unk.	2.3×10^6	[65]
113	$e^-(aq) + H_2NNH_3$	→	Unk.	2.2×10^8	[65]
114	$O^- + H_2NNH_2$	→	$OH^- + \cdot NHNH_2$	1.7×10^9	[66]
115	$H_2NNH_2 + O_3^-$	→	Unk.	1.2×10^6	[66]
116	$H_2NNH_2 + OH\cdot$	→	$H_2O + \cdot NHNH_2$	1.4×10^{10}	[65]
117	$H_2NNH_3 + OH\cdot$	→	$H_2O + \cdot N_2H_4^+$	1×10^9	[65]
118	$e^-(aq) + \cdot NO$	→	NO^-	2.3×10^{10}	[67]
119	$\cdot NO + OH\cdot$	→	$H^+ + NO_2^-$	1×10^{10}	[68]
120	$H\cdot + \cdot NO$	→	HNO	1.1×10^{10}	[69]
121	$e^-(aq) + N_2O$	→	$N_2 + O^-$	9.6×10^9	[49]
122	$H\cdot + N_2O$	→	$N_2 + OH\cdot$	2.1×10^6	[70]
123	$OH^- + NH_3OH^+$	→	$H_2O + NH_2OH$	1×10^9	Assumption
124	$H_2O + NH_2OH$	→	$OH^- + NH_3OH^+$	9.55	From $pK_a = 5.98$
125	$OH^- + H_2NNH_3$	→	$H_2NNH_2 + H_2O$	1×10^9	Assumption

Table 2.1: continued

Id.	Reactants		Products	Rate constant	Ref
126	$H_2NNH_2 + H_2O$	→	$OH^- + H_2NNH_3$	912	From $pK_a = 7.96$
127	$NO^- + O_2$	→	$ONOO^-$	2.7×10^9	[41]
128	$NO^- + \cdot NO$	→	$N_2O_2^-$	3×10^9	[71]
129	$HNO + \cdot NO$	→	$H^+ + N_2O_2^-$	5.8×10^6	[41]
130	$N_2O_2^- + \cdot NO$	→	$N_3O_3^-$	5.4×10^9	[71]
131	$N_2O_2^- + O_2$	→	$O_2^- + 2\cdot NO$	1×10^6	[72]
132	$N_3O_3^-$	→	$N_2O + NO_2^-$	300	[71]
133	$OH^- + HNO$	→	$NO^- + H_2O$	4.9×10^4	[41]
134	$NO^- + H_2O$	→	$OH^- + HNO$	120	[41]
135	2HNO	→	$H_2O + N_2O$	8×10^6	[41]
136	$\cdot NO_2 + OH\cdot$	→	ONOOH	4.5×10^9	[73]
137	ONOOH	→	$\cdot NO_2 + OH\cdot$	0.35	[73]
138	ONOOH	→	$H^+ + NO_3^-$	0.9	[73]
139	$HO_2 + \cdot NO$	→	ONOOH	3.2×10^9	[73]
140	$O_2^- + NO_3^-$	→	$NO_3^{2-} + O_2$	1×10^6	[63]
141	$O_2^- + \cdot NO$	→	$ONOO^-$	5×10^9	[73]
142	$ONOO^-$	→	$O_2^- + \cdot NO$	0.02	[73]
143	$ONOO^-$	→	NO_3^-	8×10^{-6}	[73]
144	$ONOO^-$	→	$O^- + \cdot NO_2$	1×10^{-6}	[73]
145	$O^- + \cdot NO_2$	→	$ONOO^-$	3.5×10^9	[73]
146	$NO_2^- + OH\cdot$	→	$OH^- + \cdot NO_2$	5×10^9	[68]
147	$e^-(aq) + NO_2^-$	→	NO_2^{2-}	3.5×10^9	[63]
148	$O_2^- + NO_2^-$	→	$O_2 + NO_2^{2-}$	5×10^6	[67]
149	$H_2O + NO_2^{2-}$	→	$2OH^- + \cdot NO$	4.3×10^4	[74]
150	$ONOO^- + OH\cdot$	→	$OH^- + O_2 + \cdot NO$	4.8×10^9	[73]
151	$H_2O + 2\cdot NO_2$	→	$H^+ + NO_3^- + NO_2^-$	6.5×10^7	[75]
152	$\cdot NO_2 + \cdot NO$	→	N_2O_3	1.1×10^9	[73]
153	$e^-(aq) + \cdot NO_2$	→	NO_2^-	1×10^{10}	[63]
154	$O_2^- + \cdot NO_2$	→	$O_2 + NO_2^-$	2×10^8	[74]
155	N_2O_3	→	$\cdot NO_2 + \cdot NO$	8.4×10^4	[73]
156	$N_2O_3 + ONOO^-$	→	$2\cdot NO_2 + NO_2^-$	3.1×10^8	[73]
157	$N_2O_3 + H_2O$	→	$2H^+ + 2NO_2^-$	2×10^3	[73]
158	$OH^- + N_2O_3$	→	$H_2O + 2NO_2^-$	1×10^8	[73]
159	HNO	→	$H^+ + NO_2^-$	7.24×10^7	From pKa = 3.14
160	$H^+ + NO_2^-$	→	HNO	1×10^{11}	[73]
161	$O_2 + \cdot NO$	→	$\cdot ONOO$	1×10^6	[76]
162	$\cdot ONOO$	→	$O_2 + \cdot NO$	2×10^5	[76]
163	$\cdot ONOO + \cdot NO$	→	ONOONO	5.8×10^5	[76]
164	ONOONO	→	$2\cdot NO_2$	5×10^3	[76]
165	$\cdot NH_2O_2$	→	$H_2O + \cdot NO$	6.1×10^5	This work

2.2.4 Computational details

All Quantum Chemical (QC) computations were performed using the Gaussian 09 program suite.[77] Reactant geometries were optimized using the hybrid functional UB3LYP[8,9] and the 6-31G(d) basis set. The search for the transition state (TS) was performed by first conducting a relaxed potential energy surface scan of the bond length of a bond postulated to break in the reaction (usually one of the N-H bonds). The geometry corresponding to the maximum in energy in the scan was subsequently used as a starting guess for a TS search using the Berny algorithm. The identified TS geometry was then subject to a frequency analysis and the presence of one imaginary frequency was asserted. Next, the intrinsic reaction coordinate (IRC) was followed to confirm that the TS indeed connected the reactant with a product. The end structures of the IRC scan were then also subjected to a frequency analysis

in order to enable vibrational energy corrections to be made to the reaction profile. If the obtained product was not expected to be stable, its role as an intermediate was investigated by an additional TS search toward expected product and repetition of the above steps.

Once the reactant, TS, product, possible intermediates and additional transition states of a reaction step were optimized at the UB3LYP/6-31G(d) level of theory, a refined geometry optimization was performed for each structure at the UM06-2X/6-311+G(2df,2p)/PCM level of theory. The polarizable continuum model (PCM) employed was the integral equation formalism variant and it was set to represent water.

For all reaction paths, different number of water molecules were investigated. The number of explicit water molecules used in the different cases, the number of investigated reaction paths for each case and the number of unique reaction paths are presented in table 2.2.

All converged structures from the UM06-2X/6-311+G(2df,2p) optimizations (except for some of the reaction paths involving four explicit water molecules) were then used as input for single point energy calculations at the CCSD(T)/6-31+G(d) and the UMP2/6-311+G(2df,2p) level of theory. The latter computations were used to make a basis set extrapolation similar to the G2 scheme[78] (here excluding empirical corrections). The extrapolation of the energy was made by adding the difference in energy between the two MP2 energies with large and small basis set to the CCSD(T) energy of the small basis set. The accuracy of this extrapolation was investigated by conducting computations at the CCSD(T)/6-311+G(2df,2p) level for the smaller systems.

The absorption spectrum of $H_2NOO^{\bullet}$ was calculated for a large number of optimized structures from the investigated reaction paths with varying number of water molecules using TDDFT at the UM06-2X/6-311+G(2df,2p) level of theory.

For gaining mechanistic insights in the character of the hydrogen transfer, a Natural Bond Orbitals population analysis[79] was performed for all structures at the UM06-2X/6-311+G(2df,2p) level. The detailed information of the partial spins and charges on the atoms can be found in section 2.3 in the supplementary material. Geometrical information on the NOO group can also be found for all structures at the same level of theory in section 2.4 in the supplementary material.

2.3 Results and discussion

The results from the experiments and the modeling of the homogeneous reaction system are presented in section 2.3.1. The results from the QC calculations are presented in section 2.3.2.

2.3.1 Experimental results

The evolution of the concentration of $ONOO^-$ during the simulation of the radiolysis is provided in fig. 2.6 together with the corresponding concentration evolution after

Table 2.2: Reaction paths investigated using QC. n_w denote number of explicit water molecules in the model, n_{rp} denote the number of reaction paths investigated and n_{urp} reports the same number but with the coincidentally identical paths excluded. Each reaction path consists at least of three structures (reactant, TS and product), for $n_w = 4$ some paths featured an intermediate and an associated second TS (*cf.* section 2 in the supplementary material).

Reaction	n_w	n_{rp}	n_{urp}
$NH_2OO^\bullet \rightarrow NHOOH$	0	1[a]	1
	1	2	1[b]
	2	3	3
	3	12	7
	4	33	27
$^\bullet NHOOH \rightarrow NO^\bullet + H_2O$	0	1	1
	1	1	1
	2	1	1
$NH_2OO^- \rightarrow NO^- + H_2O$	0	1[c]	1
$NH_2OOH \rightarrow^1 HNO + H_2O$	1	1	1

a) In this work only the 1,3-hydrogen shift with importance to the aqueous decomposition is investigated, for a full investigation of the PES in vacuum *cf.* ref.[30]
b) There is a very small difference between two paths, differing in the angle of the non-participating hydrogen on water with respect to the non-interacting hydrogen on nitrogen.
c) Extensive attempts were made to locate transition states with 1, 2 and 3 water molecules, however no real transition states were found on the singlet nor the triplet potential energy surface. The exception was for the case with 3 water molecules but it had a computationally divergent IRC scan associated with it.

irradiation in the γ-radiolysis experiments. One can note the non-exponential decay in the modeled case of the oxygen atmosphere (*cf.* fig. 2.6a) as well as a sub-optimal fit of an exponential function in the corresponding experimental case (*cf.* fig. 2.6c). It is also interesting to see that both of these differ qualitatively from the model (*cf.* fig. 2.6b) and experimental (*cf.* fig. 2.6d) results of the system with an oxygen deficiency. Even though the first order decays of $ONOO^-$leading to products not in direct equilibrium with it (reaction 143 and 144 in table 2.1) have a combined rate of $9 \times 10^{-6}\,s^{-1}$, we see a much faster disappearance. This is due to reaction 142 in table 2.1 which is in quasi-equilibrium with $ONOO^-$through reaction 141 in the same table. However, $NO^\bullet$ and $^\bullet O_2^-$are slowly removed from the solution by other processes which differ in rate between the two systems. Hence the fitted exponential decay is of limited value. One experimentally reoccurring feature that the model fails to reproduce is the delay observed in reaching the maximum yield of $ONOO^-$in the solutions with the highest concentrations of N_2O(*cf.* fig. 2.6d). The

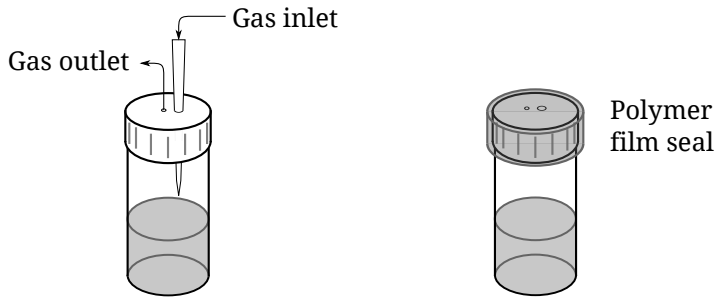

(a) Glass vial with gas inlet used for purging before irradiation.

(b) Glass vial sealed with polymer film to prevent gas dissipation.

Figure 2.5: The radiolysis experiments of aqueous ammonia employed glass vials placed at different positions (with different dose-rates) in a Cs-137 gamma radiation source. The influence of the atmosphere composition was investigated by purging the water filled vials with a O_2/N_2O gas mixture of known composition.

failure of the model in this respect is qualitative and suggests that there might be one or more non-negligible processes currently unknown.

Due to the very large reaction system the identity of the missing and/or improperly represented reactions or erroneous rate coefficient remains unknown.

The results of the resulting spectroscopically measured concentration of $ONOO^-$ in the γ-radiolysis of the aqueous ammonia solution for different lengths of irradiation are presented in fig. 2.7. We can see that the model presented in table 2.1, accurately reproduce the experiment in pure O_2. However, the agreement with the experimental data for the system with N_2O is far from satisfactory. The deviation is so large that it either suggests that some process is missing in the model, or some of the reported reactions (which include speculative elements) are in error.

The linear regression of the $ONOO^-$ yield, as a function of total dose in figs. 2.7a to 2.7c, give the effective yield, $G_{exp}(ONOO^-)$. This number is compared in table 2.3 to the effective yields of $^{\bullet}OH$ and $^{\bullet}O_2^-$ from eqs. (2.3) and (2.4) evaluated at the concentrations used in this experiment. The close agreement between $G_{exp}(ONOO^-)$ and $G_{tot}(^{\bullet}O_2^-)$ for the solutions with N_2O ($^{\bullet}OH$ in excess) suggests that $^{\bullet}O_2^-$ is efficiently converted to $ONOO^-$, while the yield in the system deficient in $^{\bullet}OH$ is considerably lower than what the simplified competition kinetics model suggests. Given the better agreement with experiment for the oxygen rich solution, this deficiency is more probably in the simplified competition kinetics analysis rather than the large model. The same analysis done to experimental yields where the total dose is varied through dose rate (*cf.* fig. 2.9) instead of irradiation time give slightly different values (*cf.* table 2.3).

The competition kinetics analysis with respect to initial NH_3 concentration both for experiment and model is presented in (*cf.* fig. 2.8). The competition kinetics analysis of this kind works best for cases where the yield is governed by the

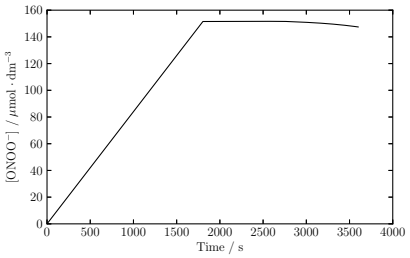

(a) Model prediction of $ONOO^-$ concentration during (0 s to 1800 s) and after (1800 s to 3600 s) irradiation of solution with $p_{O_2} = 1.0\,\text{atm}$.

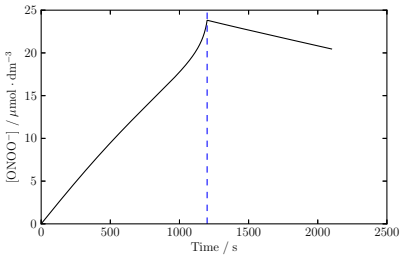

(b) Model prediction of $ONOO^-$ concentration during (0 s to 1200 s) and after (1200 s to 2400 s) irradiation of solution with $p_{O_2} = 0.2\,\text{atm}$ and $p_{N_2O} = 0.8\,\text{atm}$. The vertical dashed line marks 2400 s.

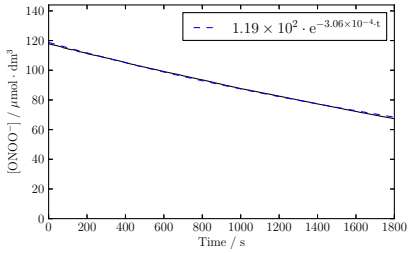

(c) Experimental $ONOO^-$ concentration with fitted exponential decay. The decomposition is measured after 30 min irradiation (time between end of irradiation and start of measurement: 40 s). $p_{O_2} = 1.0\,\text{atm}$.

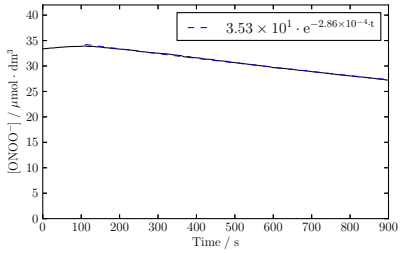

(d) Experimental $ONOO^-$ concentration with fitted exponential decay. The decomposition is measured after 20 min irradiation (time between end of irradiation and start of measurement: 60 s). $p_{O_2} = 0.2\,\text{atm}$ and $p_{N_2O} = 0.8\,\text{atm}$

Figure 2.6: The transient concentration of $ONOO^-$ after irradiation in experiment and model (model also include transient concentration during radiolysis). The two model results have the same initial conditions as the corresponding experimental data: $[NH_3] = 1.0\,\text{M}$, $[OH^-] = 20\,\text{mM}$, $\dot{D} = 0.3\,\text{Gy}\,\text{s}^{-1}$, The pressure of O_2 and N_2O varies between the data (se individual plot captions).

competition of two reactions, one between ammonia and a limiting reactant leading to $ONOO^-$, and one between the limiting reactant and another species leading to bi-products. By inspection, it looks as if there are two regions where linear fits of very different slopes are applicable. One in the low concentration regime, and one in the high concentration regime. A lot of effort was put into trying to formulate a model of such kind, however, no satisfactory formulation was found.

Table 2.3: Effective G-values from irradiation experiments ($G_{exp}(ONOO^-)$), and from competition kinetics ($G_{tot}(O_2^{\bullet -})$ and $G_{tot}(^{\bullet}OH)$) calculated according to eqs. (2.3) and (2.4) for $[OH^-] = 0.02$ Molar, $[NH_3] = 1.0$ M and $P_{tot} = 1.0$ atm, using $H_{O_2} = 1.3 \times 10^{-3}$ M atm^{-1} and $H_{N_2O} = 2.5 \times 10^{-2}$ M atm^{-1} (from ref.[80]). Limiting reactant concentrations, assuming 1:1 stoichiometric relation between formed $ONOO^-$ and respective radical, are marked red.

p_{O_2} / atm	p_{N_2O} / atm	$G_{tot}(^{\bullet}O_2^-)$ / µmol Gy^{-1}	$G_{tot}(^{\bullet}OH)$ / µmol Gy^{-1}	$G_{exp}(ONOO^-)^a$ / µmol Gy^{-1}	$G_{exp}(ONOO^-)^b$ / µmol Gy^{-1}
1.0	0.0	0.34	0.28	0.20(2)	0.25
0.5	0.5	0.099	0.52	0.105(20)	0.12
0.2	0.8	0.077	0.54	0.095(20)	-

a) Determined from total dose varied through irradiation time (*cf.* fig. 2.7). Error estimate given is twice the difference between the yields corresponding to $\dot{D} = 0.1$ Gy s^{-1} and $\dot{D} = 0.3$ Gy s^{-1}.
b) Determined from total dose varied through dose rate (*cf.* fig. 2.9).

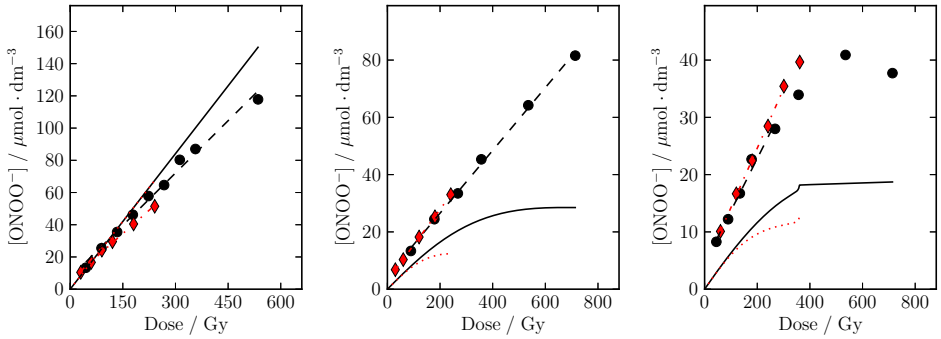

(a) 1.0 atm O_2, $G_{0.1}$=1.9, $G_{0.3}$=2.1

(b) 0.5 atm O_2, 0.5 atm N_2O, $G_{0.1}$=1.2, $G_{0.3}$=1.1

(c) 0.2 atm O_2, 0.8 atm N_2O, $G_{0.1}$=1.0, $G_{0.3}$=0.9 (only the first five data points included in linear fit)

Figure 2.7: Irradiation time-scan. G_x denotes effective radiolytic yield of $ONOO^-$ at $\dot{D} = x$ Gy s^{-1}, the value given is divided by 10^{-7} mol Gy^{-1}. ●Experimental data (0.3 Gy s^{-1}), - - - Linear fit to experimental data (0.3 Gy s^{-1}), ——— model (0.3 Gy s^{-1}), ◆ Experimental data (0.1 Gy s^{-1}), · — · — · Linear fit to experimental data (0.1 Gy s^{-1}), · · · · model (0.1 Gy s^{-1})

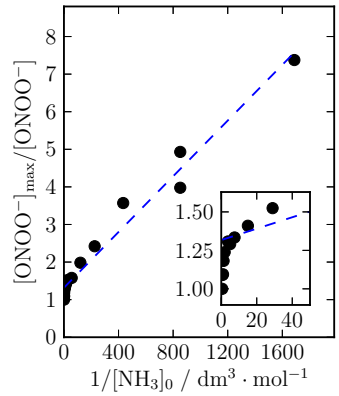

(a) 1.0 atm O_2, Experimental, Slope: 3.7×10^{-3} mol dm^{-3}

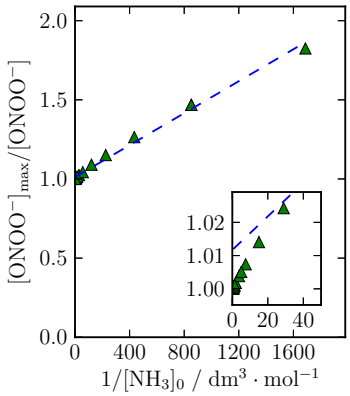

(b) 1.0 atm O_2, Model, Slope: 5.1×10^{-4} mol dm^{-3}

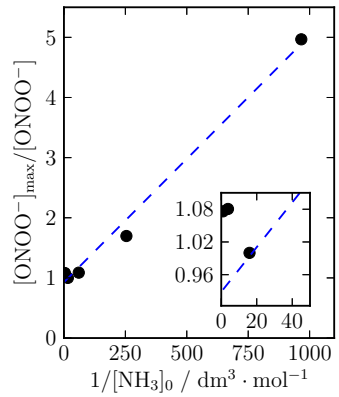

(c) 0.5 atm O_2, 0.5 atm N_2O, Experimental, Slope: 4.1×10^{-3} mol dm^{-3}

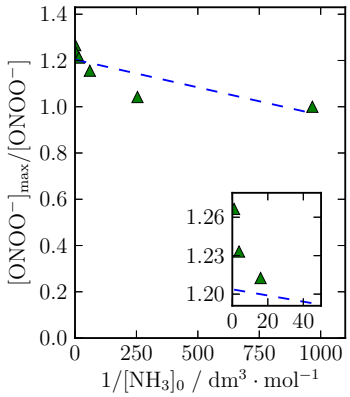

(d) 0.5 atm O_2, 0.5 atm N_2O, Model, Slope: -2.4×10^{-4} mol dm^{-3}

Figure 2.8: Competition kinetics ●Inverse yield normalized to maximum yield after 600 s irradiation with $\dot{D} = 0.3$ Gy s^{-1}, · – · – · Linear fit to inverse normalized yield. The slope of the fit is presented in the individual captions.

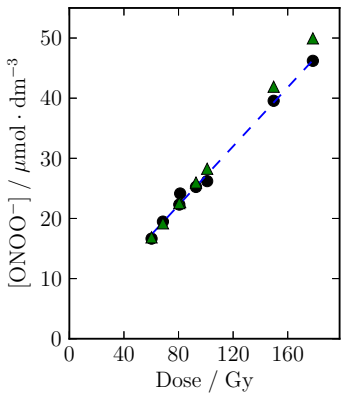

(a) 1.0 atm O_2. From linear fit: $G_{exp}(ONOO^-) = 2.5 \times 10^{-7}\,\mathrm{mol\,Gy^{-1}}$

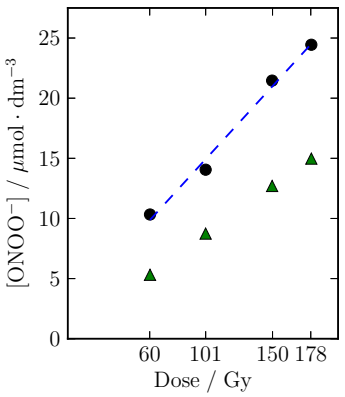

(b) 0.5 atm O_2, 0.5 atm N_2O. From linear fit: $G_{exp}(ONOO^-) = 1.2 \times 10^{-7}\,\mathrm{mol\,Gy^{-1}}$

Figure 2.9: Yield of $ONOO^-$ as function of total dose. The varied variable within each series was the dose rate, while the irradiation time was constant. ● Experimental data, ▲ Model, – – – Linear fit to experimental data. Conditions: $[OH^-] = 20\,\mathrm{mM}$, $[NH_3] = 1.0\,\mathrm{M}$

2.3.2 Computational results

The computed reaction free energies and activation free energies for the reaction paths studied are presented in section 2.3.2. The transition state structures corresponding to the lowest barrier for each step is presented in fig. 2.10. The results of the calculation of the absorption spectrum of $H_2NOO^{\bullet}$ is presented in table 2.5.

The reaction with O_2 is found to be divided into two steps corresponding to a first and a second 1,3-hydrogen migration from nitrogen to the terminal oxygen. This is in accordance with the postulated transition states. Furthermore, we see that the first step is essentially thermoneutral while the second step is exergonic. The reaction barrier is largest for the first hydrogen transfer, making it the rate determining step. By only including solvation through a PCM model the barrier merely drops $6\,\mathrm{kJ\,mol^{-1}}$, while including one explicit water molecule in the computations, the barrier drops another $53\,\mathrm{kJ\,mol^{-1}}$. Then we do not observe any dramatic effect until the fourth explicit water molecules is included. Laszlo et al.[32] observed a half-life of $H_2NOO^{\bullet}$ of about 10 µs, corresponding to an activation free energy of $45\,\mathrm{kJ\,mol^{-1}}$, a value which we only reach for the largest number of water molecules studied in this work (4). By inspecting the barrier heights for all calculated cases of water structuring in the supplementary material (*cf.* table 25 therein), we see the importance of the exhaustive sampling of the phase space. Of the 27 investigated conformers, only two are compatible with the experimental data. The same is also true for the wavelength of the absorption maximum (experimentally

Table 2.4: Summary of computed reaction energies and barriers for the four different reaction steps studied. n_{expl} denote the number of explicit water molecules added to the model, n_{invl} denote the number of water molecules directly involved in the hydrogen transfer for the reaction path with the lowest energy barriers, $\Delta G^{\ddagger}$ give the free energy of activation and ΔG_r is the free energy of the reaction step. The energies reported are the CCSD(T)/6-31+G(d)//UM06-2X/6-311(2df,2p) extrapolated to the 6-311+G(2df,2p) basis set. The energies are those of the reaction path with the lowest energy barrier for each system of n_{expl} explicit water molecules. When several reaction paths are available for a reaction step, the reported reaction path is that composed of reactant, TS and product structures of the most stable conformation (*i.e.* the structures are pooled from all reaction paths respectively).

Reaction step			n_{expl}	n_{invl}	$\Delta G^{\ddagger}$ / kJ mol^{-1}	ΔG_r / kJ mol^{-1}
$NH_2OO^{\bullet}$	$\rightarrow$	$^{\bullet}NHOOH$	-[a]	-	140	6
			0	0	134	3
			1	1	81	−5
			2	1	86	−11
			3	2	68	−3
			4	2	43	−6
$^{\bullet}NHOOH$	$\rightarrow$	$NO + H_2O$	-[a]	-	14	−319
			0	0	17	−316
			1	1	40 [b]	−294
			2	2	18 [c]	−334
NH_2OO^-	$\rightarrow$	$NO^- + H_2O$	-[a]	-	14 [d]	−166
			0	0	17 [d]	−146 [e]
NH_2OOH	$\rightarrow$	$HNO + H_2O$	1	1	55 [e]	−171

a) In vacuo (no PCM model used)
b) H transfer at $r_{OO} = 2.1\,\text{Å}$
c) OO bond cleavage at $r_{OO} = 1.6\,\text{Å}$
d) Intramolecular H transfer at $r_{OO} = 1.5\,\text{Å}$
e) HNO and OH^- is formed instead of NO^- and H_2O

Table 2.5: Computed UV/vis absorption of spectrum of $NH_2OO^\bullet$. The wave length is the average wave length of absorption associated with the largest oscillator strength in the computations. The number in parenthesis is the average value of the associated oscillator strength.

Specie	n_{expl}	λ_{max}(TD-DFT[f]) / nm	λ_{max}(EOM-CCSD[g]) / nm
$NH_2OO^\bullet \cdot nH_2O$	0	297(0.070)	209(0.079)
	1	309(0.064)	-
	2	315(0.060)	218(0.073)
	3	324(0.058)	-
	4	326(0.041)	-

f) Time dependent DFT using UM06-2X/6-311+G(2df,2p)
g) Equation-of-motion CCSD/6-311+G(2df,2p)

reported in the same paper to be around 340 nm). In this work the solvatochromic shift observed in the TDDFT results suggest that the computations are converging (even though not yet fully converged) to this experimental value with the number of water molecules. The discrepancy between the TDDFT results in comparison with the EOM-CCSD results is worrisome. Unfortunately the cost associated with EOM-CCSD computations makes further exploration of this difficult.

For the reaction between $^\bullet NH_2$ and $^\bullet O_2^-$ the computations suggests that the reaction should be competitive with the one with O_2. The reaction have never been studied experimentally, and the reason for this is that is very hard to design an experiment where sufficient $^\bullet O_2^-$ concentration can be achieved and at the same time exclude O_2. Additional complication arise in finding a reliable way of detecting the nitroxyl anion since formation of $ONOO^-$ is not longer possible due to the lack of O_2.

By inspecting the detailed energy barriers presented in section 2 in the supplementary material, we see that generally the change in barrier heights and reaction energies do not change dramatically between B3LYP (without PCM corrections) and M06-2X (with PCM corrections). Both methods, however, seem to underestimate the activation energies associated with the hydrogen transfers when compared to the CCSD(T) results.

For some of the smaller systems CCSD(T)/6-311+G(2df,2p) computations were performed to evaluate the validity of the basis set extrapolation. Through comparison with the extrapolated values (table 22 in the supplementary material) we approximate the accuracy in the extrapolation to be on the order of 2 kJ mol^{-1}, and hence justifies the use of this extrapolation.

Some structures identified as intermediates at the B3LYP/6-31G(d) level were no longer local minima at the UM06-2X/6-311+G(2df,2p)/PCM level. These inter-

mediates were then simply ignored and considered to be spurious results due to the small basis set associated with the B3LYP computations.

The results of the population analysis is presented in section 2.3 in the supplementary material. We can see that for the reaction with O_2, the reactant, $H_2NOO^{\bullet}$, has most of its spin density localized on the terminal oxygen which also has a partial negative charge. As the reaction proceeds the spin density is shifted to the nitrogen atom, as is the partial negative charge (*cf.* also fig. 1a in the supplementary material). This suggests that the nature of the hydrogen shift is not that of a simple proton transfer, the analysis suggests even a hydride shift character to the reaction. However, there are many uncertainties associated with this type of analysis and the apparent hydride character should not be given too much emphasis.

From the decomposition of $H_2NOO^{\bullet}$ we see that of the direct involvement of a water molecule is apparently the most important factor in the lowering of the reaction barrier. But from the computations with only one water molecule, we conclude that it does not suffice to include only the water molecules directly involved in the hydrogen shift. Instead, additional solvation effects seem to be provided by the extra water molecules by stabilizing the transition state. These may either be steric or electronic in nature, but it is not trivial to deduce what effect is the most important in this case.

2.4 Conclusions

We can conclude that the quantitative knowledge of the rate constants of the fundamental reactions in the radiolysis of aqueous ammonia seem to be able to reproduce experimental results for oxygenated systems. However, in superoxide deficient systems, using nitrous oxide in this work, the yield of peroxynitrite is considerably underestimated. The large size of the model makes attempts of reparametrization prohibitive.

The results of the computations for the reaction between the aminyl radical and molecular oxygen is in agreement with the experimentally observed rate of decomposition. Also the absorption spectrum of the aminyl peroxide radical is reproduced. The computational results for the reaction with the superoxide (anion) suggests that the reaction is competitive to that with molecular oxygen.

The dependence of the results from the quantum chemical computations on the chosen number of water molecules shows that a surprisingly large number of explicit water molecules are needed in the computations in order to reach experimentally compatible results. Not only do the explicit water molecules directly involved in the hydrogen transfer seem to be needed, but additional electronic and/or steric stabilization seem to be provided by the other water molecules. Also the computed absorption spectrum show the same need for explicit water molecules to be represented in the model. However, the reliability of the absorption spectrum is somewhat questionable due to large differences between computational methodologies.

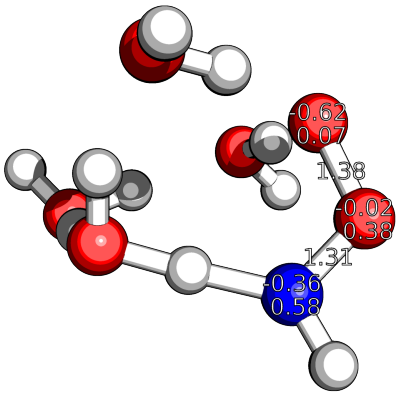

(a) $NH_2OO^{\bullet} \rightarrow {}^{\bullet}NHOOH$

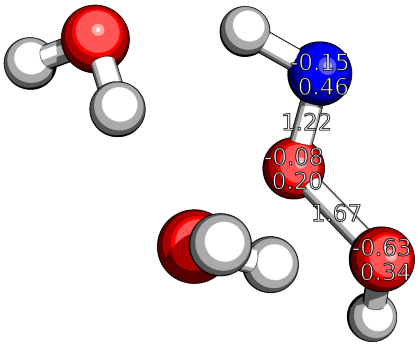

(b) ${}^{\bullet}NHOOH \rightarrow NO + H_2O$

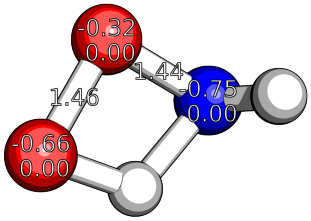

(c) $NH_2OO^{-} \rightarrow NO^{-} + H_2O$

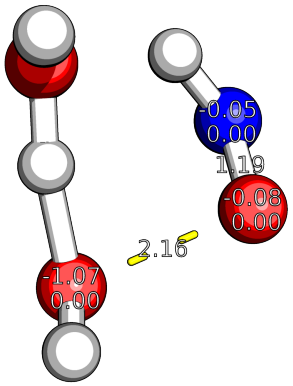

(d) $NH_2OOH \rightarrow HNO + H_2O$

Figure 2.10: Transition state structures corresponding to the lowest barrier for each step presented in section 2.3.2. Bond centered numbers give bond length in Å. Atom centered numbers give partial charge (upper) and partial spin (lower) from Natural Bond Orbital population analysis.

2.5 Acknowledgments

The author wishes to thank both of his supervisors Prof. Tore Brinck and Prof. Johan Lind, as well as Prof. Gábor Merényi for guidance and fruitful discussions throughout the work. The author is also grateful for help with computations from Joakim Halldin Stenlid and general assistance from Mats Linder.

Bibliography

(1) Jensen, F., *Introduction to Computational Chemistry*; John Wiley & Sons: 2006.

(2) Schrödinger, E. *Physical Review* **1926**, *28*, 1049, DOI: 10.1103/PhysRev.28.1049.

(3) Reiher, M.; Wolf, A., *Relativistic Quantum Chemistry*; John Wiley & Sons: 2009.

(4) Dirac, P. A. M. *Proceedings of the Royal Society of London. Series A, Containing Papers of a Mathematical and Physical Character* **1929**, *123*, 714.

(5) McQuarrie, D. A., *Quantum Chemistry*; University Science Books: 2008.

(6) Kohn, W.; Sham, L. J. *Physical Review* **1965**, *140*, A1133, DOI: 10.1103/PhysRev.140.A1133.

(7) Hohenberg, P.; Kohn, W. *Physical Review* **1964**, *136*, B864, DOI: 10.1103/PhysRev.136.B864.

(8) Becke, A. D. *J. Chem. Phys.* **1993**, *98*, 5648, DOI: doi:10.1063/1.464913.

(9) Lee, C.; Yang, W.; Parr, R. G. *Physical Review B* **1988**, *37*, 785, DOI: 10.1103/PhysRevB.37.785.

(10) O'reilly, R. J.; Karton, A.; Radom, L. *International Journal of Quantum Chemistry* **2012**, *112*, 1862–1878, DOI: 10.1002/qua.23210.

(11) Zhao, Y.; Truhlar, D. G. *Theoretical Chemistry Accounts* **2008**, *120*, 215, DOI: 10.1007/s00214-007-0310-x.

(12) Hu, C.-H.; Brinck, T. *The Journal of Physical Chemistry A* **1999**, *103*, 5379, DOI: 10.1021/jp9835061.

(13) Choppin, G.; Rydberg, J.; Liljenzin, J.-O., *Radiochemistry and Nuclear Chemistry*; Elsevier: 2001.

(14) Mozumder, A.; Hatano, Y., *Charged Particle and Photon Interactions with Matter: Chemical, Physicochemical, and Biological Consequences with Applications*; Taylor & Francis: 2003.

(15) Elliot, A.; McCracken, D. R. *Fusion Engineering and Design* **1990**, *13*, 21, DOI: 10.1016/0920-3796(90)90028-5.

(16) Tuli, J. *Nuclear Data Sheets* **1997**, *81*, 579, DOI: 10.1006/ndsh.1997.0015.

(17) Hindmarsh, A. *IMACS Transactions on Scientific Computation* **1983**, *1*, ed. by Stepleman, R., 55.

(18) Bader, G.; Deuflhard, P. *Numerische Mathematik* **1983**, *41*, 373, DOI: 10.1007/BF01418331.

(19) Marquardt, D. W. *Journal of the Society for Industrial and Applied Mathematics* **1963**, *11*, 431, DOI: 10.1137/0111030.

(20) More, J.; Garbow, B.; Hillstrom, K. User Guide for MINPACK-1., 1980.

(21) Crutzen, P. J. *Annual Review of Earth and Planetary Sciences* **1979**, *7*, 443.

(22) Gardiner, W. C. J., *Gas-Phase Combustion Chemistry*; Springer: 2000.

(23) Liochev, S. I.; Fridovich, I. *Free Radical Biology and Medicine* **1994**, *16*, 29, DOI: 10.1016/0891-5849(94)90239-9.

(24) Sharpe, M. A.; Cooper, C. E. *Biochem. J.* **1998**, *332*, 9.

(25) Silva, G. W. C.; Yeamans, C. B.; Sattelberger, A. P.; Hartmann, T.; Cerefice, G. S.; Czerwinski, K. R. *Inorganic Chemistry* **2009**, *48*, 10635, DOI: 10.1021/ic901165j.

(26) SUGIHARA, S.; IMOTO, S. *Journal of Nuclear Science and Technology* **1969**, *6*, 237, DOI: 10.1080/18811248.1969.9732878.

(27) Hack, W.; Horie, O.; Wagner, H. G. *J. Phys. Chem.* **1982**, *86*, 765, DOI: 10.1021/j100394a036.

(28) Patrick, R.; Golden, D. M. *J. Phys. Chem.* **1984**, *88*, 491, DOI: 10.1021/j150647a034.

(29) Michael, J. V.; Klemm, R. B.; Brobst, W. D.; Bosco, S. R.; Nava, D. F. *J. Phys. Chem.* **1985**, *89*, 3335, DOI: 10.1021/j100261a035.

(30) Sumathi, R.; Peyerimhoff, S. D *J. Chem. Phys.* **1998**, *108*, 5510, DOI: doi:10.1063/1.475940.

(31) Sumathi, R.; Engels, B.; Peyerimhoff, S. D *J. Chem. Phys.* **1996**, *105*, 8117, DOI: doi:10.1063/1.472666.

(32) Laszlo, B.; Alfassi, Z. B.; Neta, P.; Huie, R. E. *J. Phys. Chem. A* **1998**, *102*, 8498, DOI: 10.1021/jp981529+.

(33) Clarke, K.; Edge, R.; Johnson, V.; Land, E. J.; Navaratnam, S.; Truscott, T. G. *J. Phys. Chem. A* **2008**, *112*, 1234, DOI: 10.1021/jp076395r.

(34) Menkin, V.; Makarov, I.; Pikaev, A. *Klum. Vyska Energy* **1991**, *25*, 60.

(35) De Laat, J.; Boudiaf, N.; Dossier-Berne, F. *Water Research* **2010**, *44*, 3261, DOI: 10.1016/j.watres.2010.03.009.

(36) Li, J.; Blatchley III, E. R. *Environ. Sci. Technol.* **2009**, *43*, 60, DOI: 10.1021/es8016304.

(37) Pagsberg, P. B.; Eriksen, J.; Christensen, H. C. *J. Phys. Chem.* **1979**, *83*, 582, DOI: 10.1021/j100468a006.

(38) Neta, P.; Maruthamuthu, P.; Carton, P. M.; Fessenden, R. W. *J. Phys. Chem.* **1978**, *82*, 1875, DOI: 10.1021/j100506a004.

(39) Mikhailova, T. L.; Ershov, B. G. *Russian Chemical Bulletin* **1993**, *42*, 235, DOI: 10.1007/BF00697066.

(40) Pouchan, C.; Lam, B.; Bishop, D. M. *J. Phys. Chem.* **1987**, *91*, 4809, DOI: 10.1021/j100302a032.

(41) Shafirovich, V.; Lymar, S. V. *Proc. Natl. Acad. Sci.* **2002**, *99*, 7340, DOI: 10.1073/pnas.112202099.

(42) Hughes, M. N.; Nicklin, H. G. *Journal of the Chemical Society A: Inorganic, Physical, Theoretical* **1968**, 450, DOI: 10.1039/j19680000450.

(43) Dahlgren, B. PyKinetics., 2012.

(44) Eigen, M.; De Maeyer, L. *Zeitschrift für Elektrochemie, Berichte der Bunsengesellschaft für physikalische Chemie* **1955**, *59*, 986–993, DOI: 10.1002/bbpc.19550591020.

(45) Perrin, D. D; International Union of Pure and Applied Chemistry. Commission on Equilibrium Data, *Ionisation constants of inorganic acids and bases in aqueous solution*; Pergamon Press: Oxford [Oxfordshire]; New York, 1982.

(46) Bielski, B. H. J.; Cabelli, D. E.; Arudi, R. L.; Ross, A. B. *Journal of Physical and Chemical Reference Data* **1985**, *14*, 1041, DOI: doi:10.1063/1.555739.

(47) Buxton, G.; Clive, L; Greenstock, W; Helman, P; Ross, A. *J. Phys. Chem. Ref. Data* **1988**, *17*, 513.

(48) Elliot, A. J.; Corrosion, C. R. L. S. C. a., *Rate Constants and G-values for the Simulation of the Radiolysis of Light Water Over the Range 0-300C*; Chalk River Laboratories, Fuel Engineering Branch: 1992.

(49) Elliot, A. J. *International Journal of Radiation Applications and Instrumentation. Part C. Radiation Physics and Chemistry* **1989**, *34*, 753, DOI: 10.1016/1359-0197(89)90279-8.

(50) Sehested, K.; Holcman, J.; Bjergbakke, E.; Hart, E. J. *J. Phys. Chem.* **1982**, *86*, 2066, DOI: 10.1021/j100208a031.

(51) Boyd, A.; Carver, M.; Dixon, R. *Radiation Physics and Chemistry (1977)* **1980**, *15*, 177, DOI: 10.1016/0146-5724(80)90129-6.

(52) Sehested, K.; Holcman, J.; Bjergbakke, E.; Hart, E. J. *J. Phys. Chem.* **1984**, *88*, 269, DOI: 10.1021/j150646a021.

(53) Buehler, R. E.; Staehelin, J.; Hoigne, J. *J. Phys. Chem.* **1984**, *88*, 2560, DOI: 10.1021/j150656a026.

(54) Staehelin, J.; Buehler, R. E.; Hoigne, J. *J. Phys. Chem.* **1984**, *88*, 5999, DOI: 10.1021/j150668a051.

(55) Staehelin, J.; Hoigne, J. *Environmental Science & Technology* **1982**, *16*, 676, DOI: 10.1021/es00104a009.

(56) Pagsberg, P. *Aspects of Research at Risø* **1972**, *5*, 209.

(57) Lind, J.; Merényi, G. *The Journal of Physical Chemistry A* **2006**, *110*, 192, DOI: 10.1021/jp054747t.

(58) Hoigne, J; Bader, H; Haag, W.; Staehelin, J *Water Research* **1985**, *19*, 993, DOI: 10.1016/0043-1354(85)90368-9.

(59) Hickel, B.; Sehested, K. *International Journal of Radiation Applications and Instrumentation. Part C. Radiation Physics and Chemistry* **1992**, *39*, 355, DOI: 10.1016/1359-0197(92)90244-A.

(60) Menkin, V.; Makarov, I.; Pikaev, A. *High Energy Chem* **1988**, *22*, 333.

(61) Schwarz, H. A. *J. Phys. Chem.* **1991**, *95*, 6697, DOI: 10.1021/j100170a058.

(62) Yakabuskie, P. A.; Joseph, J. M.; Clara Wren, J. *Radiation Physics and Chemistry* **2010**, *79*, 777, DOI: 10.1016/j.radphyschem.2010.02.001.

(63) Yakabuskie, P. A.; Joseph, J. M.; Stuart, C. R.; Wren, J. C. *The Journal of Physical Chemistry A* **2011**, *115*, 4270, DOI: 10.1021/jp200262c.

(64) Simic, M.; Hayon, E. *Journal of the American Chemical Society* **1971**, *93*, 5982, DOI: 10.1021/ja00752a005.

(65) Hayon, E.; Simic, M. *Journal of the American Chemical Society* **1972**, *94*, 42, DOI: 10.1021/ja00756a008.

(66) Ershov, B.; Mikhailova, T. *Bull. Acad. Sci. USSR, Div. Chem. Sci.* **1991**, *40*, 288.

(67) Seddon, W. A.; Young, M. J. *Canadian Journal of Chemistry* **1970**, *48*, 393, DOI: 10.1139/v70-063.

(68) Loegager, T.; Sehested, K. *J. Phys. Chem.* **1993**, *97*, 6664, DOI: 10.1021/j100127a016.

(69) Knight, R. J.; Sutton, H. C. *Transactions of the Faraday Society* **1967**, *63*, 2628, DOI: 10.1039/TF9676302628.

(70) Czapski, G.; Peled, E. *Isr. J. Chem.* **1968**, *6*, 421.

(71) Lymar, S. V.; Shafirovich, V.; Poskrebyshev, G. A. *Inorganic Chemistry* **2005**, *44*, 5212, DOI: 10.1021/ic0501317.

(72) Poskrebyshev, G. A.; Shafirovich, V.; Lymar, S. V. *The Journal of Physical Chemistry A* **2008**, *112*, 8295, DOI: 10.1021/jp803230c.

(73) Goldstein, S.; Lind, J.; Merényi, G. *Chem. Rev.* **2005**, *105*, 2457, DOI: 10.1021/cr0307087.

(74) Goldstein, S.; Czapski, G. *Inorganic Chemistry* **1996**, *35*, 5935, DOI: 10.1021/ic960438t.

(75) Cortas, N. K.; Wakid, N. W. *Clinical Chemistry* **1990**, *36*, 1440.

(76) Goldstein, S.; Czapski, G. *Journal of the American Chemical Society* **1995**, *117*, 12078, DOI: 10.1021/ja00154a007.

(77) Frisch, M. J.; Trucks, G. W.; Schlegel, H. B.; Scuseria, G. E.; Robb, M. A.; Cheeseman, J. R.; Scalmani, G.; Barone, V.; Mennucci, B.; Petersson, G. A. *Inc., Wallingford, CT* **2009**, *2*, 4.

(78) Curtiss, L. A.; Redfern, P. C.; Smith, B. J.; Radom, L. *J. Chem. Phys.* **1996**, *104*, 5148, DOI: doi:10.1063/1.471141.

(79) Reed, A. E.; Curtiss, L. A.; Weinhold, F. *Chem. Rev.* **1988**, *88*, 899, DOI: 10.1021/cr00088a005.

(80) Lide, D. R., *Handbook of Chemistry and Physics*; CRC Press: 1995.